

Reversible constitutional switching between macrocycles and polymers induced by shape change in a dynamic covalent system†‡

Sébastien Ulrich,^a Eric Buhler^b and Jean-Marie Lehn^{*a}

Received (in Montpellier, France) 2nd October 2008, Accepted 2nd December 2008

First published as an Advance Article on the web 16th January 2009

DOI: 10.1039/b817261g

We report here the development of morphological switches as a new tool that can be used in constitutional dynamic chemistry (CDC) to control the constitution of the whole dynamic system. Molecules that have well-defined but switchable shapes were designed and synthesized. Their restrained conformational states were characterized both in the solid and in solution. The addition of metal ions induces a shape change through coordination; the shape generated was also fully investigated both in the solid and in solution. Such molecules constitute morphological switches, meaning that they can explore various shape states as a result of controlled well-defined shape changes triggered by an effector. These morphological switches were then integrated into covalent dynamic systems through formation of reversible imine bonds. Thermodynamic and kinetic analyses were performed in order to quantify the covalent equilibrium and to investigate the labile character of the covalent reversible link. It was then demonstrated that the molecular shape state of the morphological switches induces a well-defined constitution through covalent self-assembly, and that the system can be steered, quantitatively and reversibly without significant fatigue, between two different constitutional states, respectively, polymeric and macrocyclic assemblies. The dynamic covalent polymeric assemblies were analysed by DOSY NMR and small angle neutrons scattering (SANS). Their dynamic behaviour as a function of the concentration and the temperature was demonstrated and characterized.

Introduction

Constitutional dynamic chemistry (CDC)¹ investigates the generation and the behaviour of dynamic systems, self-assembled through either reversible covalent bonds² or supramolecular interactions,³ and capable of undergoing constitutional variation in response to the pressure of physical or chemical effectors. It opens the path towards complex adaptive self-organized matter.⁴ The understanding of molecular and supramolecular chemical evolution of matter in response to various stimuli offers great opportunities in various fields ranging from materials chemistry to drug research. Thus, dynamic materials⁵ have recently emerged as adaptive materials whose properties can be altered *via* a change in constitution. Dynamic combinatorial chemistry (DCC)⁶ allows for constitutional evolution at the covalent level in the presence of a biological target, thus providing information about molecular recognition processes and leading ultimately to

the discovery of biologically active⁷ or catalytically active molecules.⁸ Such investigations point to the establishment of constitution–function relationships that underlie structure–activity correlations in both materials chemistry and biomolecular science.

In synthetic systems, recent studies have shown that constitution can impact the mechanical⁹ or optical¹⁰ properties of dynamic materials at the covalent level. Various stimuli have been shown to affect the constitution of dynamic systems. Those encompass medium effect,^{11–13} concentration,^{13,14} phase change (gel formation,¹⁵ crystallization¹⁶), the application of an electric field¹⁷ and hydrostatic pressure.¹⁸

The shape of molecules is a crucial parameter in a self-assembly process. Molecular shape can modulate recognition events¹⁹ and conversely recognition events can also influence molecular shape in an induced-fit fashion.²⁰ Ultimately, it is expected that molecular morphology can strongly influence the constitution of dynamic systems, thus representing a new stimulus inducing constitutional change.

The template effect^{21,22} has been used in many systems to preorganize a molecule around an effector. This confers to the complex a well defined shape which will favour, in the next step, the selective formation of a specific product.²³ Typically, macrocycles are efficiently formed by using such a synthetic methodology which prevents the competitive formation of polymeric products.²⁴ Shape affects a separated generation of polymers and macrocycles in alkene metathesis processes templated by a metal ion.²⁵ Supramolecular assemblies also display shape-dependent constitution,²⁶ especially in systems

^a Laboratoire de Chimie Supramoléculaire, Institut de Science et d'Ingénierie Supramoléculaires (ISIS), 8 allée Gaspard Monge, 67083 Strasbourg, France. E-mail: lehn@isis.u-strasbg.fr; Fax: +33 (0)390 245 140

^b Laboratoire Matière et Systèmes Complexes (MSC), UMR CNRS 7057, Université Paris Diderot-Paris 7, Bâtiment Condorcet, 75205 Paris cedex 13, France

† Dedicated to Jean-Pierre Sauvage on the occasion of his 65th birthday.

‡ Electronic supplementary information (ESI) available: 2D NMR, MS characterizations, kinetic studies, SANS and DOSY NMR. CCDC reference numbers 703869–703876. For ESI and crystallographic data in CIF or other electronic format see DOI: 10.1039/b817261g

where noncovalent macrocycles and polymers can compete.²⁷ In these cases, molecular shape was controlled, among the many possible switching units,²⁸ by a photo-switchable group.

We report here that a morphological switch, involving metal-ion controlled interconversion between two states of different shapes, can reversibly steer *in situ* the constitution of covalent dynamic systems between polymers and macrocycles.²⁹ The versatility of this strategy is illustrated by the implementation in two different systems, the first carrying out reversible

switching between an organic polymer and a metallo-macrocycle, while the second one displays interconversion between a cross-linked metallo-polymer and an organic macrocycle (Scheme 1). Macrocycles and polymers are especially interesting since they represent two correlated states of a dynamic system,³⁰ which display markedly different properties.

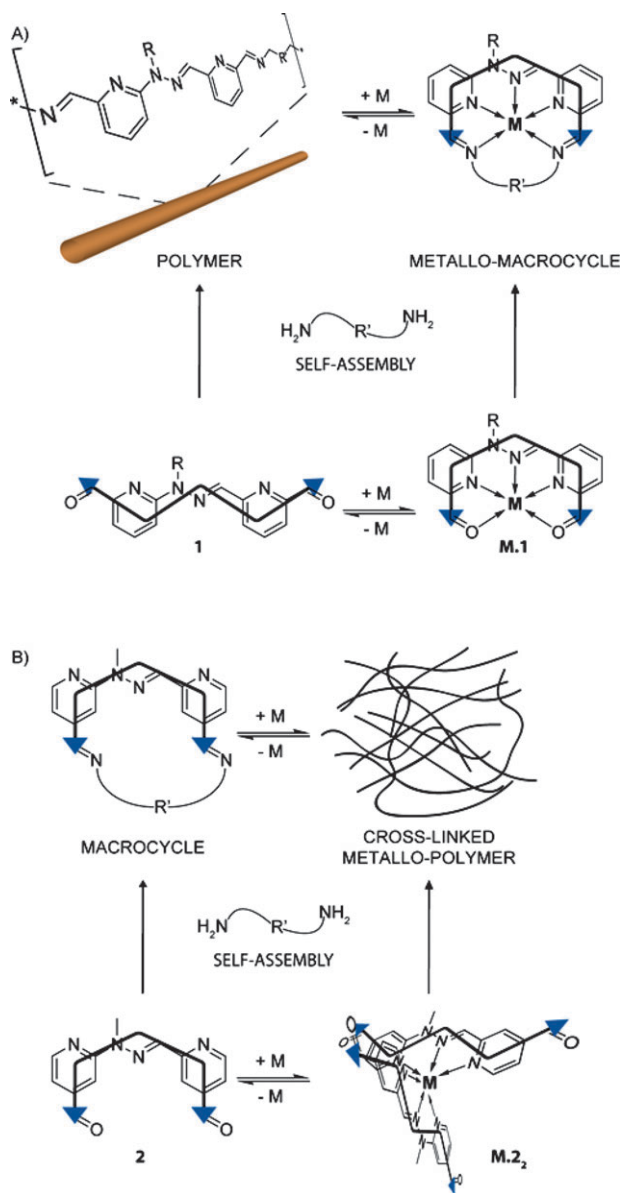
The design of the morphological switches investigated here is based on a metal ion coordinating core involving a tridentate chelating unit based on the sequence pyridine-hydrazone-pyridine, which is isomorphous to 2,2':6',2''-terpyridine.^{31,32} This group was fitted with aldehyde groups in either α (compound **1**) or γ (compound **2**) position with respect to the pyridyl nitrogens, so that in their free, uncomplexed form, compounds **1** and **2** define, respectively, an extended W-shaped state and a compact U-shaped state. On binding of a metal ion, reorientation of the pyridine groups switches the shape, respectively, to a U and a W state in the complexed core (Scheme 1 and Fig. 4). Such type of ligands have been previously used to perform contraction/extension molecular motions³³ and in switchable molecular tweezers³⁴ undergoing shape change on binding of a metal ion. The aldehyde functions in **1** and **2** enable them to connect to amines present in their environment through a reversible formation of a covalent imine bond.^{35–37} Such a reversible covalent link allows for the study of the relationship between the shape-state of the morphological switch and the molecular constituent generated by condensation with diamines. One would expect that an extended W shape would favour polymer formation whereas a compact U shape, where the aldehyde groups are in close proximity, would favour macrocycle formation on condensation with a suitable diamine.²⁹ As demonstrated here, the shape switching process can induce a transient disassembly of imine bonds, which can then reassemble generating the constitution that fits best the new morphological constraints. In such systems, the self-assembly processes are thus correlated and controlled by the shape states of the morphological switches.

Results and discussion

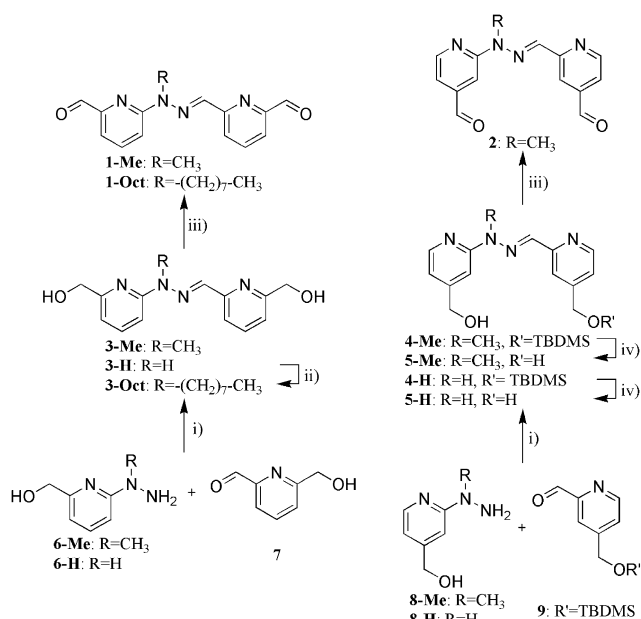
Ligand syntheses

Ligands **1** and **2** were obtained by connecting functionalized pyridine hydrazines and pyridine aldehydes bearing CH_2OH groups through a quantitative and smooth hydrazone formation (Scheme 2). At this stage, the alcohol functions can be used to covalently attach different groups. The corresponding aldehydes **1** and **2** were obtained in quantitative yield by Dess–Martin oxidation.³⁸ In the case of **3**, an alkylation method was developed in order to attach an alkyl chain to improve the solubility of some assemblies generated by imine formation (see below). It also gives access to more functionalized derivatives of such molecules. Following the same procedure, alkylation of **5-H** was tried but, albeit the product was observed by LC-MS analysis, we were unable to isolate it in a pure form. Noteworthy, this general synthetic strategy allows the construction of dissymmetric ligands, as illustrated for example by the preparation of **4**.

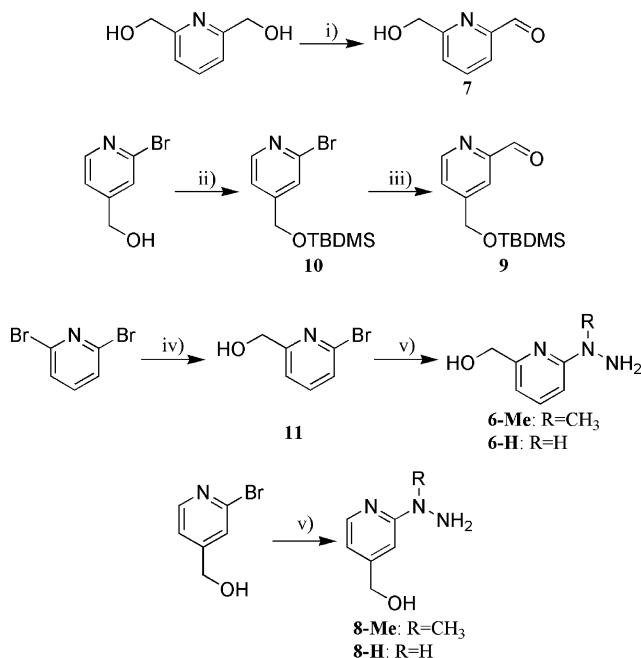
The synthetic route to the pyridine aldehydes and pyridine hydrazines building blocks is depicted in Scheme 3.



Scheme 1 Schematic representations of the principle of constitutional switching processes between macrocycles and polymers in response to W–U shape changes. A: reversible switching between a polyimine polymer and a metallo-macrocycle; B: reversible switching between an imine macrocycle and a cross-linked metallo-polymer. “+M” refers to the addition of a metal salt and “–M” refers to the addition of a competitive metal ion binder thus resulting in the sequestration of the metal ion. The stick represents the fact that the polymers formed are of rigid rod type.



Scheme 2 Synthesis of the morphological switches **1** and **2** through hydrazone formation. (i) CHCl₃, RT, 77–84%; (ii) NaH, 1-bromooctane, DMF, RT, 70%; (iii) Dess–Martin periodinane, CHCl₃, RT, quantitative; (iv) TBAF, THF, 0 °C, 81%-quantitative. TBDMS = *tert*-butyldimethylsilyl; TBAF = tetrabutylammonium fluoride.



Scheme 3 Synthesis of the pyridine aldehydes and pyridine hydrazines building blocks. (i) MnO₂, CHCl₃, 64%; (ii) TBDMS-Cl, DMAP, CH₂Cl₂, 0 °C, 93%; (iii) *n*-BuLi, DMF, THF, −78 °C, 75%; (iv) *n*-BuLi, DMF, NaBH₄, THF, −78 °C → RT, 82%; (v) methylhydrazine or hydrazine monohydrate, reflux, quantitative. TBDMS = *tert*-butyldimethylsilyl; DMAP = *N,N*-dimethyl-4-aminopyridine; BuLi = butyllithium; DMF = dimethylformamide; THF = tetrahydrofuran.

Monooxidation of commercial 2,6-pyridinedimethanol using manganese dioxide gave the dissymmetric aldehyde **7**. Aldehyde **9** was obtained in two steps from (2-bromopyridin-4-yl)methanol.

Protection of the alcohol with a silyl group gave **10**. Formylation of **10** by a bromine–lithium exchange followed by addition of DMF then yielded aldehyde **9**. The hydrazone counterparts were obtained by a substitution of the bromine-containing derivatives by the appropriate hydrazine. In summary, molecules **1** and **2** are readily accessible through the described convergent synthesis in 3 to 5 steps with overall yields ranging from 38 to 69% and straightforward purifications.

Shape of the free and complexed switching units **1** and **2**

The shape of the ligands **1** and **2** as well as of their complexes was investigated in the solid state by X-ray crystallography. The solid state molecular structure of **1-Me**, which was previously reported,²⁹ clearly shows the W shape as expected on the basis of previous studies^{31,33,34,39} and quantum mechanical calculations.⁴⁰ It is assumed that **1-Oct** has the same shape since the central pyridine–hydrazone–pyridine core is the same as in **1-Me**. Single crystals of metal complexes **M-1-Me** were obtained by slow diffusion of diisopropylether into a CHCl₃–CH₃CN solution. X-Ray crystallographic analyses revealed the solid state structure of these metal complexes and clearly show their U shape (Fig. 1). In all cases, the coordination geometry is based on an in-plane-coordination of three nitrogens complemented by two oxygens from the aldehyde groups. This feature explains why in this case, no ML₂-type (M: metal, L: ligand) species are formed when the ligand is titrated with the metal salt (see below). The additional coordination sites in the two axial positions are occupied by counter-ions completing the coordination sphere.

Whereas single crystals of **2** could not be obtained, synthetic precursors such as **4-Me** and **4-H** gave single crystals suitable for X-ray diffraction by slow evaporation of a CHCl₃ solution. Crystallographic analyses showed that the molecule presented the U shape, indicating that **2** must also have a U shape since the core of these molecules is the same (Fig. 1). Single crystals of **Pb-2** were also obtained by slow diffusion of diisopropylether into a CHCl₃–CH₃CN solution of the metal complex and X-ray diffraction analysis revealed that the ligand had a W shape as expected. The coordination sphere is made of the three nitrogens from the ligand, the two counter-anions and two additional molecules of water, forming a distorted pentagonal bipyramid.

The shapes of the ligand molecules were also studied in solution by NMR spectroscopy techniques. Since the central hydrazone makes the ligands dissymmetric, it is possible to observe NOE correlation between the two pyridine rings. Full assignment was done by using ¹H–¹³C heteronuclear HSQC and HMBP methods (ESI†). ¹H–¹H homonuclear COSY and ROESY methods showed NOE correlations between H₁ and H₂ and between H₆ and H₇ indicating that ligands **1** and **2** also have a well defined structure in solution similar to their solid state structures (Scheme 4 and ESI†).

COSY and ROESY analyses of the zinc complexes showed the typical sequence H₇–H₁–H₂–H₆ of NOE correlations⁴¹ (ESI†), demonstrating that the ligands in the metal complexes had undergone shape switching on metal binding (Scheme 4). Noteworthy, H₈ presents NOE correlations with both H₇ and H₉; H₅ also presents NOE correlations with both H₄ and H₆ in

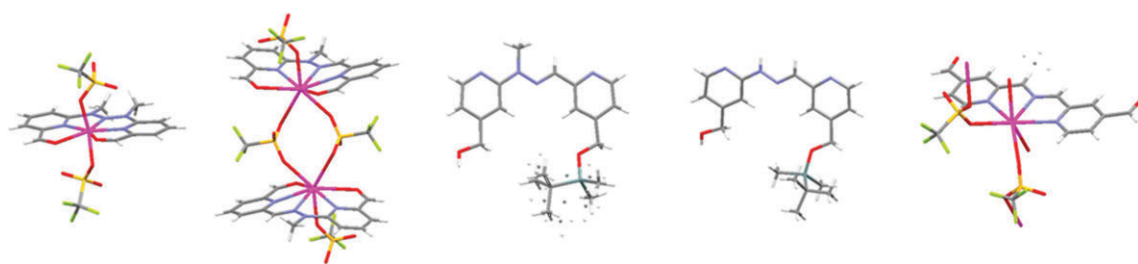
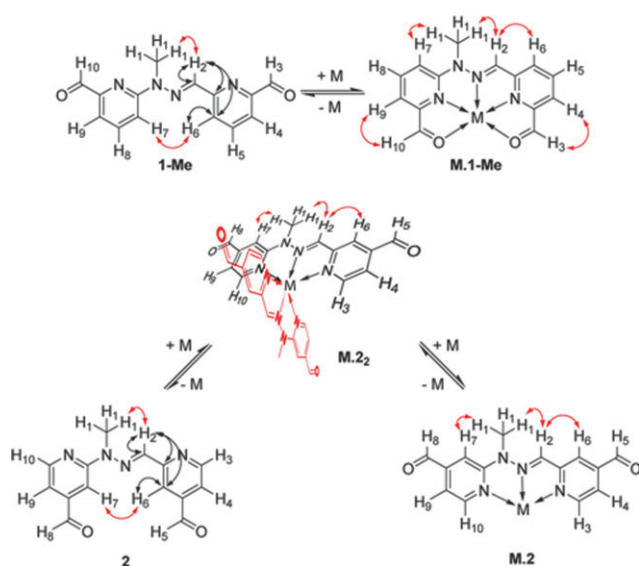


Fig. 1 Solid state molecular structures obtained from X-ray crystallography of metal complexes **M-1-Me**, ligands **4-Me** and **4-Me** and metal complex **Pb-2** showing their respective shapes. In the case of **Zn-1-Me** and **Pb-2**, disorder is present at the hydrazone functionality and both complexes have crystallographically imposed two-fold symmetry. In the case of **4-Me**, disorder is present at the *tert*-butyl group.



Scheme 4 Shape switching processes of ligands **1-Me** and **2** triggered by addition-removal of metal ions. Representation of the most important correlations observed by 2D NMR: black arrows represent ^1H - ^{13}C heteronuclear correlations whereas red arrows represent ^1H - ^1H homonuclear ones. “M” refers to the metal ion Zn(II) or Pb(II) .

2 showing that the aldehyde groups can freely rotate. Such behaviour is in strong contrast with **M-1-Me** where the position of the aldehyde groups is restricted due to the coordination of the metal ion (see below).

^1H NMR titration represents a useful way to investigate the nature of the complexation processes in solution. A typical example is shown in Fig. 2 by the titration of **1-Me** by zinc triflate in CDCl_3 - CD_3CN (6 : 4).

Two different compounds, the ligand and the complex, are observed during the titration, in slow exchange on the NMR time-scale. Thermodynamic equilibrium was reached within the time needed to take a NMR spectrum after addition of the metal salt. The linear conversion of the ligand to a new product gives support to the formation of only one kind of metal complex. In addition, the conversion is complete at 1.0 equiv. of metal ion, therefore demonstrating the formation of the ML-type complex. Contrary to what is usually observed for such a tridentate ligand,⁴² no ML_2 -type complex is observed here. This is explained by the presence of the two aldehydes which can provide, as seen in the solid state structure described above, additional binding sites for the ML-type complex.

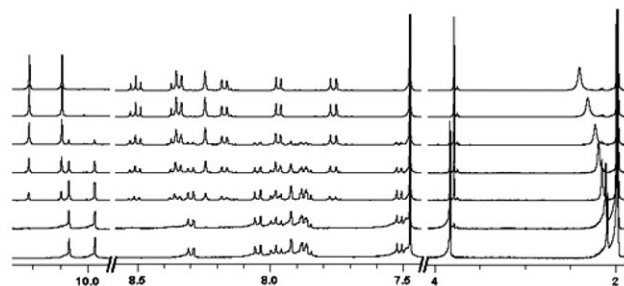


Fig. 2 ^1H NMR titration of **1-Me** by Zn(OTf)_2 in CDCl_3 - CD_3CN (6 : 4). From bottom to top: 0.0, 0.1, 0.3, 0.5, 0.7, 0.9, 1.0 equiv. of zinc triflate.

On the other hand, ligand **2** is a typical tridentate ligand which should present first a ML_2 -type complex, then a ML-type complex when titrated with a metal ion such as zinc with a strong octahedral coordination preference. The ^1H NMR titration of a solution of **2** by zinc triflate in CDCl_3 - CD_3CN (6 : 4) is shown in Fig. 3. It shows that the species formed are in slow equilibrium on the NMR time-scale and that, indeed, a new species is quantitatively formed at 0.5 equiv. of metal ion and another one after addition of 1.0 equiv. of zinc triflate. Such behaviour is typical of a tridentate ligand which first goes through a ML_2 -type complex before forming a ML-type complex at 1.0 equiv. of metal ion. Further indication of the ML_2 -type nature of the intermediate product is given by a complete analysis of the change of chemical shifts along the titration. Both complexes were analysed by 2D COSY and ROESY NMR in order to fully assign all peaks. Interestingly, it was found that the only protons which experience an up-field shift on going from **2** to **Zn-2** are H_6 and H_7 (Fig. 4). This can be attributed to the fact that their chemical shifts are situated at a low field in the free ligand due to intramolecular hydrogen bond interactions with the hydrazone sp^2 nitrogen. This observation is further indication that **2** has a U shape in solution. Such hydrogen bonds are disrupted when the structural switching occurs on metal binding, thus giving rise to an up-field shift of these protons. Among the other peaks in the aromatic region, all are shifted down-field along the titration of **2** by zinc triflate except H_2 , H_3 and H_{10} . These chemical shift changes must reflect some geometrical characteristics. Indeed, the up-field shift of H_3 and H_{10} in **Zn-2** compared to free **2** is in line with a ring current effect⁴³ induced by one ligand on the other one. These protons then undergo a classical down-field shift on

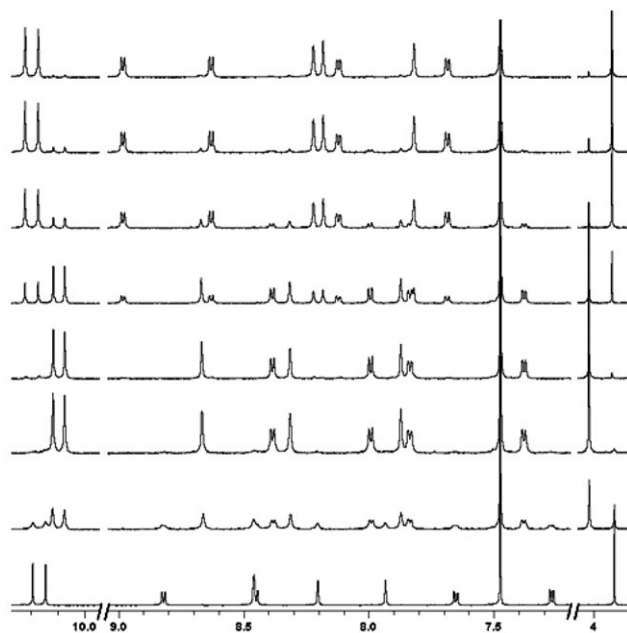


Fig. 3 ^1H NMR titration of **2** by $\text{Zn}(\text{OTf})_2$ in $\text{CDCl}_3\text{-CD}_3\text{CN}$ (6 : 4). From bottom to top: 0.0, 0.3, 0.4, 0.5, 0.6, 0.8, 0.9, 1.0 equiv. of zinc triflate.

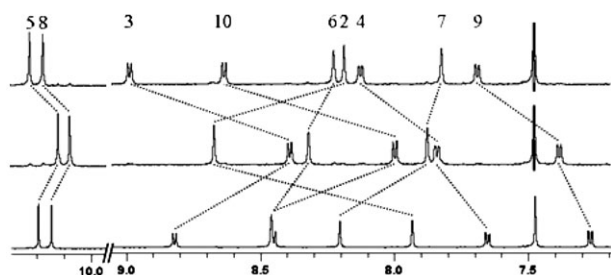


Fig. 4 ^1H NMR spectra of **2**, Zn-2 and Zn-2 , respectively, from bottom to top in $\text{CDCl}_3\text{-CD}_3\text{CN}$ (6 : 4). The numbers at the top indicate the assigned proton (see Scheme 4).

conversion of Zn-2 to Zn-2 by subsequent addition of metal ions. Changes in the chemical shift of H_2 , and even H_1 , can also be explained by a ring current effect but, since in this case the protons lie in the same plane as the second ligand, they experience a strong down-field shift on going from **2** to Zn-2 (Fig. 4).

A related behaviour can also be observed when comparing the ^1H NMR spectra of ligand **1-Me** and its zinc complex Zn-1-Me , where the signals of H_6 and H_7 are the only ones undergoing an up-field shift on the titration (Fig. 5). The other proton signals display a general down-field shift which is expected since the complexation reduces the electron density on the rings. All these data provide strong evidence about the binding mode of ligands **1** and **2** in their zinc(II) complexes.

Titration of the same ligands by lead triflate revealed that the species formed are in fast equilibrium on the NMR time scale, in contrast to the cases discussed above for zinc(II). Thus, titration of **1-Me** by lead triflate indicated a continuous conversion of the starting dialdehyde into a new compound whose formation was complete at 1.0 equiv. of metal ion

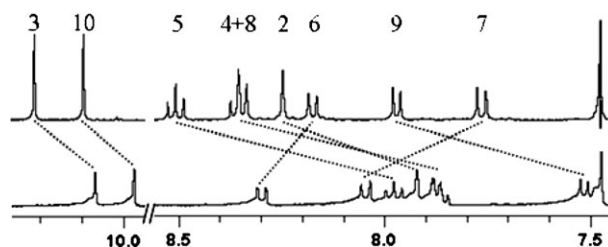


Fig. 5 ^1H NMR spectra of **1-Me** and Zn-1-Me , respectively, from bottom to top. The numbers at the top indicate the assigned proton (see Scheme 4).

(Fig. 6). In contrast, but in agreement with the previous discussion, titration of **2** by lead triflate displayed an inflexion point in the chemical shift evolution of the dialdehyde resonance peaks at around 0.5 equiv. of metal ion added (Fig. 7), pointing to the formation of a ML_2 -type complex, which is thereafter converted to a ML -type complex at 1.0 equiv. of metal ion, as indicated by the lack of chemical shift change upon addition of further metal ion. It is noteworthy that the only peaks that experience an up-field shift along the titration are those attributed to H_6 and H_7 (see discussion above).

In order to evaluate the interaction between these ligands and the metal ions used, titrations of the ligands were monitored by UV-visible spectroscopy. Titration of **1-Me** by zinc triflate clearly shows a closely linear conversion up to the formation of a plateau at 1.0 equiv. of metal ion. On the other hand, titration of **2** by zinc triflate shows an inflection point at 0.5 equiv. of metal ion indicating, like NMR spectroscopy did, the presence of an intermediate complex (Fig. 8 and 9).

Titrations performed with lead triflate seem to show the same kind of processes although information about the stoichiometry of the complexes cannot be directly deduced (ESI†).

Taken together, all these data show the formation of only the ML -type complex when ligand **1-Me** is titrated with either

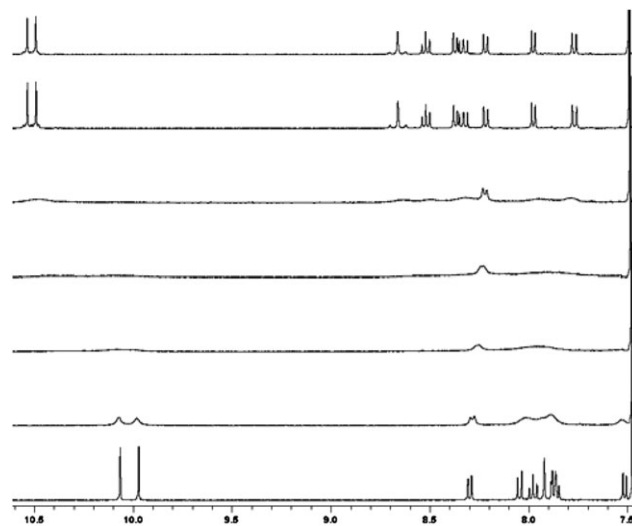


Fig. 6 ^1H NMR titration of **1-Me** by $\text{Pb}(\text{OTf})_2$ in $\text{CDCl}_3\text{-CD}_3\text{CN}$ (6 : 4). From bottom to top: 0.0, 0.1, 0.3, 0.5, 0.7, 0.9, 1.0 equiv. of lead triflate.

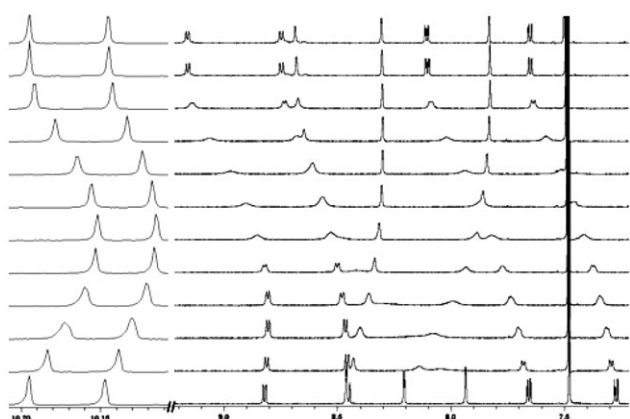


Fig. 7 ^1H NMR titration of **2** by $\text{Pb}(\text{OTf})_3$ in $\text{CDCl}_3\text{-CD}_3\text{CN}$ (6 : 4). From bottom to top: 0.0, 0.1, 0.2, 0.3, 0.4, 0.5, 0.6, 0.7, 0.8, 0.9, 1.0, 1.5 equiv. of lead triflate. The scale between the two parts of the spectra is different in order to emphasize the change of chemical shifts of the aldehyde peaks along the titration.

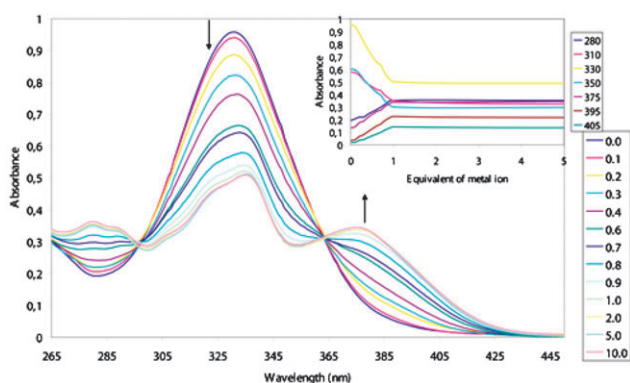


Fig. 8 UV-visible titration of **1-Me** by zinc triflate in $\text{CHCl}_3\text{-CH}_3\text{CN}$ (6 : 4). The inset shows the evolution of the absorbance along the titration at different wavelengths.

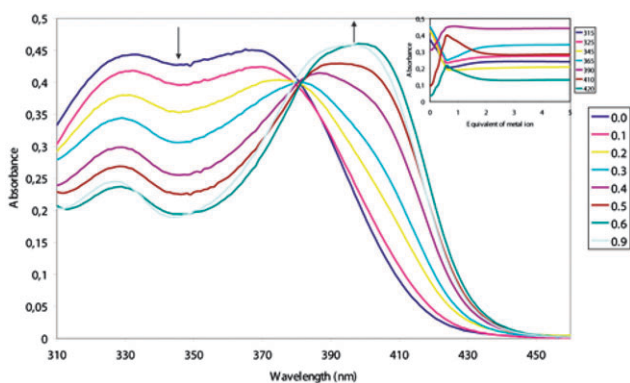


Fig. 9 UV-visible titration of **2** by zinc triflate in $\text{CHCl}_3\text{-CH}_3\text{CN}$ (6 : 4). The inset shows the evolution of the absorbance along the titration at different wavelengths.

zinc or lead ions whereas ligand **2** shows formation of a ML_2 -type complex and a ML -type complex with both metal ions. Treating UV-visible spectroscopy data with Letagrop software⁴⁴ with these complexation models allowed a gross evaluation of the associations constants, which were however

Table 1 Approximate association constants for the formation of metal complexes

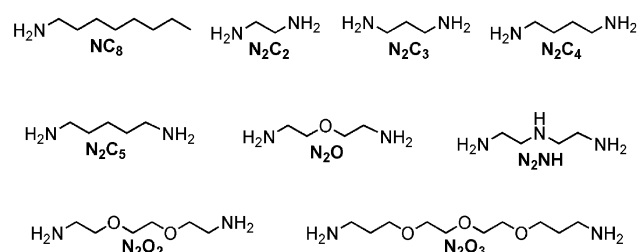
Ligand	Metal salt	$\text{Log}_{10}K_{11}^a$	$\text{Log}_{10}\beta^b$
1-Me	$\text{Zn}(\text{OTf})_2$	> 8	—
1-Me	$\text{Pb}(\text{OTf})_2$	≈ 7	—
2	$\text{Zn}(\text{OTf})_2$	> 8	> 14
2	$\text{Pb}(\text{OTf})_2$	≈ 5	≈ 10

^a K_{11} refers to the equilibrium between ligand, metal salt and the ML -type complex. ^b β refers to the equilibrium between ligand, metal salt and the ML_2 -type complex.

in line with data on terpy as ligand (Table 1).⁴² The association constants of the lead complexes are always smaller than their zinc equivalent.

In summary, the data presented show that ligands **1** and **2** have well-defined W and U shapes, respectively, both in solid state and in solution. Moreover, their shapes can be switched to the other one by addition of a metal ion. Ligand **2** can yield two types of complexes according to the amount of metal salt added. Furthermore, addition of hexacyclen to the zinc complexes and cryptand [2.2.2] to the lead complexes results in the complete decomplexation due to formation of more stable metal complex with these complexing agents.⁴⁵ Therefore, a shape change can be reversibly triggered by addition of metal ion or its removal by addition of a better binder. Such systems therefore operate as ion-controlled morphological switches.

Imine formation: thermodynamic and kinetic analysis. The morphological switches **1** and **2** were appended with aldehyde functions in order to give access to dynamic covalent processes by imine formation with amines in the environment. The reversible condensation of amines with carbonyl groups to imines represents a particularly attractive interconversion and has been extensively implemented in dynamic covalent/molecular chemistry.^{35,46} In our cases, as it will be shown thereafter, hemiaminal intermediates were not detected. That means that dehydration of hemiaminal was much faster than addition of the amine onto the aldehyde moiety under our conditions ($\text{CHCl}_3\text{-CH}_3\text{CN}$ mixtures).



Imine formation at thermodynamic equilibrium was studied using UV-visible spectroscopy. Titration of **2** by *n*-octylamine **NC**₈ in $\text{CHCl}_3\text{-CH}_3\text{CN}$ (6 : 4) displays changes in the absorption spectrum (Fig. 10). Analytical treatment with the Letagrop software⁴⁴ gave the equilibrium constant by assuming a two-step model with formation of two different imines, $\text{log}_{10}K_{11} = 5.7 \pm 0.2$ and $\text{log}_{10}\beta = 8.4$. As reference, titration of pyridine-2-carboxaldehyde by *n*-octylamine **NC**₈ under the same conditions also led to changes in the absorption spectra

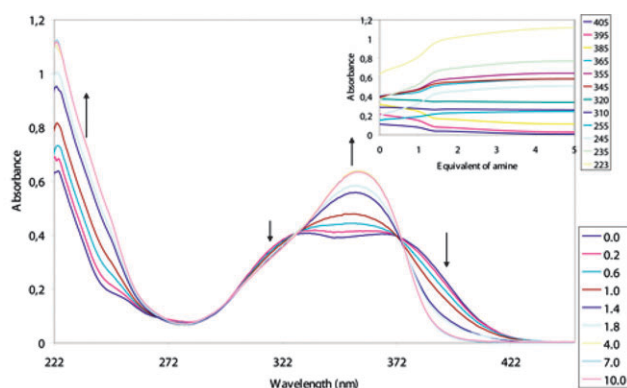


Fig. 10 Titration of **2** by *n*-octylamine **NC₈** in CHCl_3 – CH_3CN (6 : 4) monitored by UV-visible spectroscopy. The inset shows the evolution of the absorbance along the titration at different wavelengths.

which yielded $\log_{10}K_{11} = 4.6 \pm 0.3$. Both cases show that in CHCl_3 – CH_3CN mixtures imine formation between a pyridine aldehyde and an alkylamine occurs with an equilibrium constant of roughly 10^5 , which is quite high¹² and probably reflects the activation of the aldehyde by the electron-withdrawing pyridine.⁴⁷

Following imine formation by ^1H NMR spectroscopy, two intermediates were detected as two additional methyl (*ca.* 3.9 ppm) and aldehyde peaks were observed (*ca.* 9.8 and 10.3 ppm) in the spectra of **1-Me** and **2** after the addition of **NC₈** (ESI†). Since the central hydrazone unit makes the ligand dissymmetric, the two aldehyde groups should have a different reactivity and their products of single condensation are not equivalent, yielding two different monoaldehyde–monoimine intermediates (ESI†).

Integration of the NMR peaks gave the evolution of the concentration of each species *versus* time after addition of **NC₈** to **1-Me** (Fig. 11) or to **2** (ESI†).

The time-dependent concentration curves could be fitted by using first-order rate equations with correlation coefficients always greater than 0.97 (ESI†). Although the reaction must formally be of second order, the initial excess of amine (2.0 equiv.) per aldehyde function makes it about pseudo-first order.^{48,49} A control experiment performed with an excess of amine (20 equiv.) confirmed the pseudo-first order with respect to the dialdehyde. The observed pseudo-first order rate constants thus obtained (Table 2) allow comparison of structural effects on the imine formation rate.

From these data, it can be seen that imine formation is much faster with dialdehyde **1-Me** than with its isomer **2**, the first one undergoing imine formation *ca.* 5 times faster than the second one. This rate difference may either reflect differences of reactivity (LUMO levels)⁴⁷ between pyridine-2-carboxaldehyde and pyridine-4-carboxaldehyde or may be due to the formation of a transient hydrogen bond between the free amine and the pyridine nitrogen that would result in an increase in the rate of imine formation.

There is also a difference in reactivity between the two aldehyde groups in the starting material, which is much more pronounced in the case of **1-Me** than in the case of **2** *i.e.* intermediate 1 is formed *ca.* 1.3 times faster than intermediate 2 in the former case, as compared to a factor of 1.1 in the latter

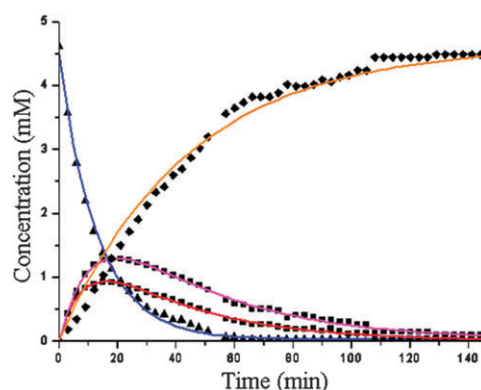


Fig. 11 Plot of the evolution of the concentration of species after addition of 2.0 equiv. of *n*-octylamine to **1-Me**. The triangles represent the starting dialdehyde, the diamonds represent the final diimine and the two other curves represent the two intermediates. The fits were obtained by using pseudo-first order kinetic equations (see text and ESI†).

case. This difference can also be observed when comparing the difference in chemical shifts between the two aldehyde peaks in the ^1H NMR spectrum of the starting dialdehyde (0.09 ppm in **1-Me** and 0.05 ppm in **2**), reflecting that the effect of the hydrazone on the dissymmetrization of the ligand is more pronounced in **1-Me** than in **2**. The difference of reactivity between the **1-Me** and **2** regarding imine formation is in contrast with their similar thermodynamic composition at equilibrium. After addition of 1.0 equiv. of **NC₈** to the starting dialdehyde, composition at equilibrium is, in the case of **1-Me**, 22% of the starting dialdehyde, 28% of intermediate 1, 22% of intermediate 2 and 28% of diimine **1-(NC₈)₂** and, in the case of **2**, 21% of the starting dialdehyde, 27% of intermediate 1, 23% of intermediate 2 and 29% of diimine **2-(NC₈)₂**.⁵⁰ Again, we can observe an imbalance between the two sides of the same dialdehyde which is due to the dissymmetrization effect of the central hydrazone, which therefore affects both kinetic and thermodynamic parameters.

Reaction of dialdehyde **2** with 1,5-diaminopentane **N₂C₅** forms quantitatively the corresponding [1 + 1] macrocycle, as demonstrated by ^1H NMR spectroscopy and mass spectrometry (see below). Following the condensation in the same conditions as previously described, no intermediate was observed by ^1H NMR, showing that the second imine formation is much faster than the first one. The formation of the cyclic diimine is thus somewhat 30 times faster than the formation of non-cyclic ones (Table 2). Transimination^{22,36} occurred under the same conditions, addition of 1,5-diaminopentane to non-cyclic diimine **2-(NC₈)₂**, and resulted in the complete conversion, driven by a chelate-type effect, of the latter to the corresponding cyclic diimine with an observed pseudo-first order constant almost similar to the direct condensation of 1,5-diaminopentane onto **2** (Table 2). No catalyst was required for such exchange to proceed using CDCl_3 – CD_3CN mixtures as medium.^{37,49}

The labile character of imines is, of course, a required character to develop covalent dynamic libraries, but can also be a major drawback, in particular regarding their characterization, so that freezing/locking⁵¹ the reaction, either by pH change⁵² or by reduction,⁵³ is usually performed. Interestingly,

Table 2 Observed pseudo-first order rate constants (min^{-1}) and related half-reaction time (min) for the condensation of amines onto dialdehydes **1** and **2** and diimine **2-(NC₈)₂**

Starting material	Amine	Intermediate 1	Intermediate 2	Diimine	$t_{1/2}^a$	$t_{1/2}^b$
1-Me	NC₈	0.115 (6)	0.090 (4)	0.023 (1)	9.1	30.1
2	NC₈	0.024 (1)	0.022 (2)	0.0044 (2)	43.3	157.5
2	N₂C₅	0.126 (4)		0.126 (4)	5.5	5.5
2-(NC₈)₂	N₂C₅	0.099 (8)		0.099 (8)	7.0	7.0

^a Refers to the disappearance of the starting material. ^b Refers to the appearance of the product.

whereas ESI mass spectrometry was not satisfactory, probably due to the break of the imines in the dilute conditions used, the imine assemblies could be directly analysed by MALDI-TOF mass spectrometry using a neutral matrix. (See ESI†)

Formation of macrocycles with the U-shaped core unit. Since a U-shaped molecule places two functions close together in space, it is expected that it would favour macrocycle formation with a diamine molecule.

Reaction of dialdehyde **2** with 1,2-diaminoethane, 1,3-diaminopropane or 1,4-diaminobutane gave [2 + 2] macrocycles, as shown by the following data. Addition of 1,2-diaminoethane to **2** resulted in the formation of a precipitate with no starting material left in solution (¹H NMR). Analysis of the precipitate by MALDI-TOF mass spectrometry⁵⁴ revealed the presence of only the [2 + 2] macrocycle (ESI†). Addition of 1,3-diaminopropane to **2** gave a crystalline product for which X-ray crystallographic analysis revealed the structure of the [2 + 2] macrocycle (Fig. 12). This macrocycle forms columns through stacking of the pyridine rings creating a central void defining channels filled by solvent molecules. Analysis of the crystals by MALDI-TOF mass spectrometry confirmed the [2 + 2] macrocyclic structure (ESI†). Addition of 1,4-diaminobutane to **2** yielded macroscopic ribbons (Fig. 13) with no starting material left in solution. Direct analysis of this solid product by MALDI-TOF also demonstrated the formation of the [2 + 2] macrocycle.

This assembly was found to be soluble in CDCl₃. The ¹H NMR spectrum was then recorded at different concentrations ranging from 5 to 50 mM. The changes in chemical shift

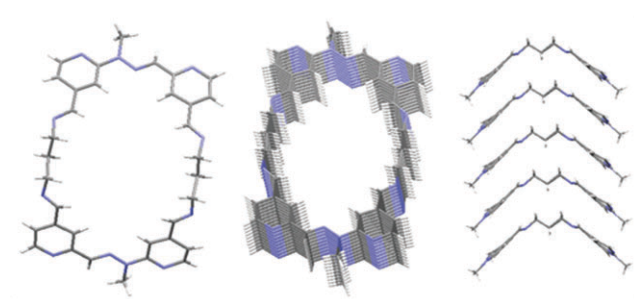


Fig. 12 Solid state structure of **2-(N₂C₅)₂** spontaneously formed by mixing **2** and **N₂C₅** in CDCl₃–CD₃CN (6 : 4). From left to right: macrocycle alone, top view of stacked macrocycles forming a column, side view of a column. Solvent molecules were present inside the cavity and removed for clarity. While the macrocycle has crystallographically imposed two-fold symmetry, there is extensive disorder of both the macrocycle and included solvent. The mean aromatic–aromatic distances are in the range 3.46–3.53 Å. It is noteworthy that the product presents an *anti* configuration of the hydrazones with respect to each other in the macrocycle.

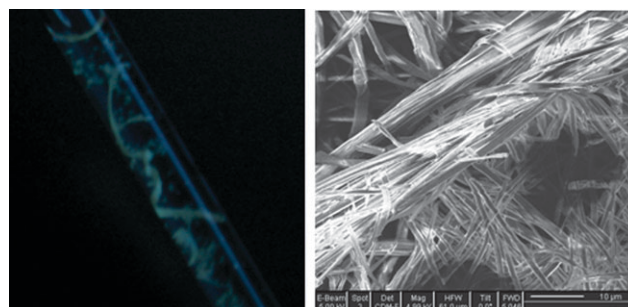


Fig. 13 Photograph showing the macroscopic ribbon formed in an NMR tube after reaction of **2** and **N₂C₄**, yielding the [2 + 2] macrocycle **2-(N₂C₄)₂** (left) and SEM picture of the material (right).

tend to show that this aggregation through π – π stacking also occurs in solution state to some extent (ESI†). The [1 + 1] macrocycle was obtained with 1,5-diaminopentane **N₂C₅** whereas [2 + 2] macrocycles were formed with 1,5-diamino-3-oxapentane in a CDCl₃–CD₃CN (6 : 4) solution, as shown by ¹H NMR spectroscopy and MALDI-TOF mass spectrometry (Fig. 14). The fact that **N₂C₅** is the only diamine of the tested series leading to the formation of a [1 + 1] macrocycle and not to a [2 + 2] one, probably reflects the better fit between the diamine length and the distance between the two aldehyde groups in **2**.

Metallo-macrocycles were formed through double imine condensation that took times ranging from minutes to a few hours depending on the diamine added to the metal complexes **M-1** in CDCl₃–CD₃CN mixtures. The solid state structures (see above) show that distances between the aldehyde carbons are 11.7 Å in **1-Me**, 6.5 Å in **Pb-1-Me** and 5.2 Å in **Zn-1-Me**. Thus, addition of 1,4-diaminobutane, 1,5-diaminopentane, 1,5-diamino-3-oxapentane onto **Zn-1** afforded the corresponding [1 + 1] macrocycles whereas 1,2-bis(2-aminoethoxy)ethane and

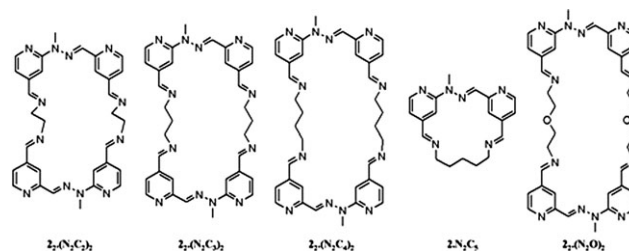


Fig. 14 Macrocycles formed from self-assembly through imine formation between **2** and various diamines. It is noteworthy that the [2 + 2] macrocycles are expected to be mixtures of *syn* and *anti* products with respect to the relative position of the hydrazone.

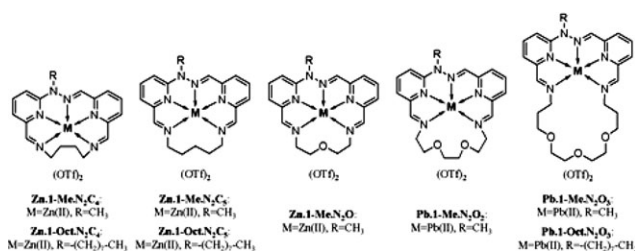


Fig. 15 Metallo-macrocycles formed from self-assembly through imine formation between **1-Me** and various diamines.

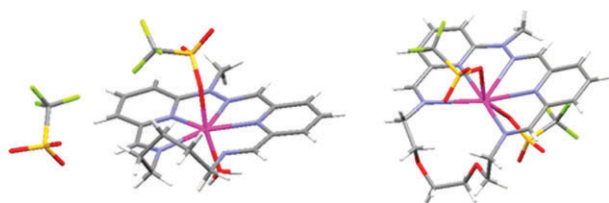


Fig. 16 Solid state structures of metallo-macrocycles **Zn-1-Me-N₂C₅** (left) and **Pb-1-Me-N₂O₂** (right) self-assembled from their components through imine formation. In the second case, the oxygens from the chain lie at 3.06 and 4.36 Å indicating that an additional weak coordination exists between one oxygen atom and the central lead ion.

4,7,10-trioxa-1,13-tridecanediamine reacted with **Pb-1** to afford the corresponding [1 + 1] macrocycles (Fig. 15).

These metallo-macrocycles were characterized by NMR spectroscopy and MALDI-TOF mass spectrometry as well as by X-ray crystallography for some of them. **1-Me** and zinc triflate gave preferentially the [1 + 1] macrocycles with the short diamines **N₂C₄** and **N₂C₅**, whereas the longer diamines **N₂O₂** and **N₂O₃** yielded a mixture of products. In contrast, with lead triflate, **1-Me** provided cleanly the [1 + 1] macrocycles with the longer diamines **N₂O₂** and **N₂O₃**. These results reflect both the larger distance between the aldehyde groups in **Pb-1-Me** than in **Zn-1-Me** and the ability of the larger lead(II) cation to accommodate various coordination geometries, as shown by the crystal structure of **Pb-1-Me-N₂O₂** (Fig. 16).

In addition to the solid state structure of **Zn-1-Me-N₂C₄**, which has been previously described,²⁹ the crystal structures of **Zn-1-Me-N₂C₅** and **Pb-1-Me-N₂O₂** (Fig. 16) were determined by X-ray diffraction on single crystals obtained by slow diffusion of diisopropylether into a $\text{CHCl}_3\text{-CH}_3\text{CN}$ solution of the metal complex. They both confirm the structure of the [1 + 1] metallo-macrocycles. The two oxygens from the chain in **Pb-1-Me-N₂O₂** lie at 3.06 and 4.36 Å from the central lead ion suggesting that the first one interacts weakly with the metal ion. The corresponding distance can be compared with the five nitrogen–lead distances, which range from 2.62 to 2.90 Å.

Polymer formation with the W-shaped core unit. The outcome of a self-assembly is highly dependent on preorganization, *i.e.* on the structural fit between the shape of the starting material and the final entity generated.⁵⁵ The 1 : 1 condensation of a W-shaped dialdehyde and a α,ω -diamine is therefore expected to lead to the formation of imine polymers, because the two aldehyde functions are held far apart from each other and thus favouring linear poly-association rather

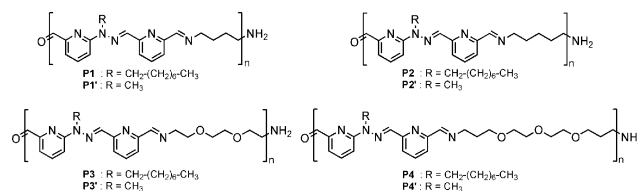


Fig. 17 Molecular structures of the polymers studied.

than cyclization (Fig. 17).⁵⁶ At low concentration, reaction of a W-shaped dialdehyde **1** with a diamine yielded mostly cyclic species whereas increasing the concentration then led indeed to the formation of polymeric entities.

¹H NMR spectroscopy analyses clearly showed concentration-dependent spectra for the equilibrium states of the condensation of W-shaped dialdehydes **1** and various diamines (Fig. 18 and ESI†).

As one may expect, at low concentration macrocyclic species are preferentially formed. Increasing the concentration allows the competitive formation of polymeric assemblies (see below), which become the major products at concentrations of 50 mM and above (Fig. 18 and ESI†). Since these self-assembled covalent polymers are all dynamic species,⁵⁷ dilution and concentration experiments were performed and confirmed the ability of reversibly changing the constitution by simply varying the concentration of the solution. Concentration thus represents a parameter that can be used to affect the constitution of the dynamic system. Eventually, in neat conditions, films were obtained whose mechanical characteristics are given in Table 3.

The use of alkyl diamines compared to ethylene oxide diamines makes the film rigid and even breakable, whereas the functionalization of the W-shaped dialdehyde with a C8 chain in **1-Oct** significantly lowers the glass transition temperature of the film obtained (Table 3). It is noteworthy that **P4** has a viscoelastic behaviour and display self-healing properties.^{57,58} Two pieces of freshly cut film self-heal in a few hours when put together at room temperature without the need of applying permanent pressure.

The macrocyclic or polymeric nature of the assemblies were demonstrated by combining MALDI-TOF mass spectrometry, DOSY NMR spectroscopy and small angle neutrons scattering (SANS) as discussed thereafter.

MALDI-TOF mass spectrometry of 5 mM solutions of equimolar mixtures of W-shaped dialdehydes **1** and diamines

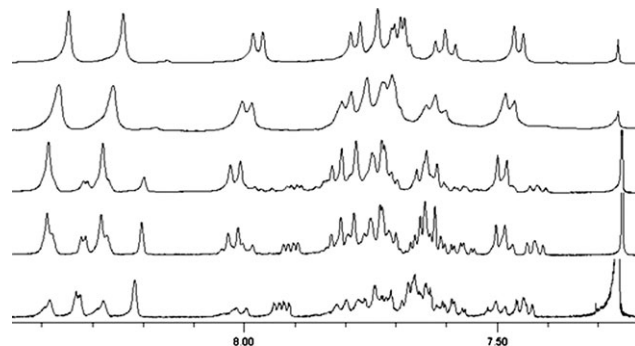
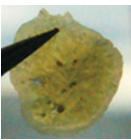
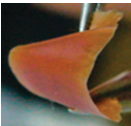




Fig. 18 ¹H NMR spectra of the self-assembly between **1-Me** and **N₂O₃** in 1 : 1 ratio at different concentrations (from bottom to top: 5, 25, 50, 100 and 200 mM) in CDCl_3 .

Table 3 Features of the polymers investigated

Polymer	Glass transition temperature/°C	Film characteristics at room temperature	Photograph of the obtained film
P1	—	Rigid	
P2	26.5	Rigid, breakable	
P4	−9.9	Stretchy	
P4'	26.0	Rigid, not breakable	

reveals masses corresponding to the [1 + 1] and [2 + 2] macrocycles (see ESI†). In some cases, higher masses corresponding to acyclic oligomers were detected, indicating the presence, in small amount, of oligomeric assemblies even at such a concentration.

DOSY NMR allows the *in situ* separation and identification of objects depending on their diffusion coefficients, which are related to object size through the Einstein–Stokes relationship.⁵⁹ DOSY studies were thus performed at different concentrations on the assembly between **1-Me** and N_2O_3 . At a 5 mM concentration, molecular species of 16.4 Å diameter ($D = 490 \mu\text{m}^2 \text{s}^{-1}$) were detected, a size compatible with the molecular structure of [2 + 2] macrocycles. Increasing the concentration up to 50 mM yields much larger objects of 80 Å diameter ($D = 100 \mu\text{m}^2 \text{s}^{-1}$). DOSY analysis of the same sample three weeks later showed even larger objects of 200 Å diameter ($D = 40 \mu\text{m}^2 \text{s}^{-1}$), suggesting the occurrence of aggregation possibly by π – π stacking between the aromatic units as observed in the crystal structure of **1-Me** and in the formation of channels in **2**·(N_2C_3)₂ (see above). Indeed, ^1H NMR shows that the aromatic signals are slightly shifted up-field as the concentration is increased (Fig. 18), a change compatible with aromatic–aromatic stacking, thus adding further support towards a slow aggregation behaviour.

SANS represents a useful tool to investigate polymers and their characteristics in solution. SANS measurements were performed on CDCl_3 solutions of the polyimines **P4**, **P2** and **P4'**. At low concentration, *i.e.* 5 mM, the scattering curves characterized by a very weak intensity level showed no dependence on the scattering vector q (data not shown), indicating a

non-aggregation behaviour in line with the formation of small macrocyclic species. On the other hand, analyses performed on more concentrated solutions undoubtedly revealed polymeric species. Fig. 19 displays the scattering patterns for **P4** solutions at various concentrations (50, 77, and 100 mM) at $T = 25^\circ\text{C}$. For clarity the representation $I(q) \times C$ was chosen to shift the curves with respect to each other. Scattering curves of **P2** and **P4'** solutions can be found in the ESI†. All of the scattering curves exhibited the same overall behaviour, characterized by the following sequence: a Guinier regime in the low- q range associated with the finite size of the scattering objects followed by a regime in which the q -dependence of the scattered intensity can be described by a power law with an exponent close to -1 . At high q , we do not observe any cross-sections of the polymer, indicating that there is no lateral aggregation and thus that the polymer is made of a single chain as shown later on by the determination of the linear density of the polymers.

The data obtained at low- q can be fitted by the following expression:^{60,61}

$$\frac{1}{I(q)} = \frac{1}{I(0)} \left(1 + q^2 \frac{R_G^2}{3} \right) \quad (1)$$

where R_G is the radius of gyration of the scattering objects. The inset of Fig. 19 shows a typical plot of $1/I$ vs. q^2 obtained for $C = 50$ mM and the best fit of the data using eqn (1). The extrapolation to zero- q of the scattering intensity, $I(0)$, provides a measurement of the weight average molecular weight of the particle, M_W (see Experimental section). Table 4 shows the R_G and M_W values determined for all concentrations and cases.

At large q values, the scattering curves can be fitted satisfactorily by a locally rigid rod model. In Fig. 19 is also presented an example of fit realized by means of the des Cloizeaux law⁶² derived for rigid rod particles and valid for

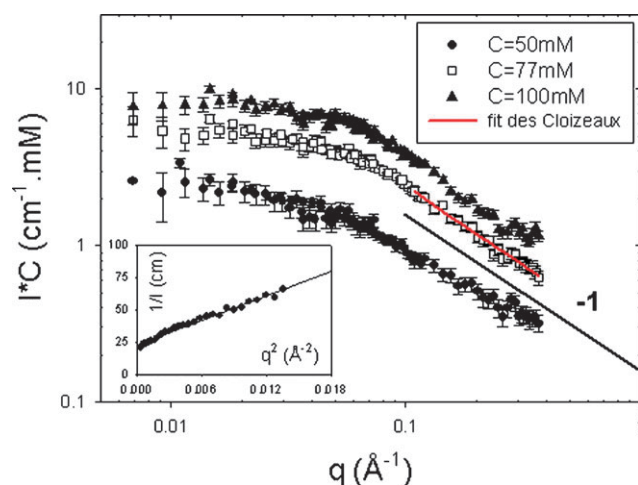


Fig. 19 Scattering patterns for **P4** solutions in deuterated chloroform at various concentrations at $T = 25^\circ\text{C}$. For clarity, the representation $I(q) \times C$ was chosen to shift the curves with respect to each other. The continuous red line represents the fit of the data in the high q -range using eqn (2). The inset shows the variation of $1/I$ with q^2 for a 50 mM sample.

Table 4 Effect of the concentration and the temperature on the radius of gyration, R_G , the weight average molecular weight, M_W , the contour length, L , and the degree of polymerization

Polymer	$T/^\circ\text{C}$	Concentration/ mM	$R_G/\text{\AA}$	$M_W/\text{g mol}^{-1}$	$L/\text{\AA}$	DP_W
P4	25	50	20.4	2200	70.7	4.0
Dehydrated P4	25	50	25.0	2472	86.6	4.5
P4	25	77	19.2	2291	66.5	4.2
P4	25	100	18.2	2053	62.9	3.7
P4	52.3	50	22.4	1705	77.5	3.1
P4	52.3	77	16.9	1486	58.7	2.7
P4	52.3	100	15.8	1160	54.6	2.1
Dehydrated P4	60	100	15.8	1867	54.7	3.4
P2	25	50	22.2	2375	77.0	5.5
P2	25	100	20.8	2491	71.9	5.8
P4'	25	100	22.8	1776	78.9	3.9
P4'	25	200	17.1	1289	59.2	2.8

$qL_p > 2$, where L_p is the persistence length and L the contour length.

$$P(q) = \frac{\pi}{qL} + \frac{2}{3q^2L_pL} \quad (2)$$

By fitting the above equation (eqn (2)) to the experimental data, one can determine the mass per unit length of the fibrillar aggregates, M_L . From the fit of Fig. 19, one obtains $M_L = 31 \text{ g mol}^{-1} \text{\AA}^{-1}$ —a value in agreement with linear mass density of a single polymer chain, which can be estimated using the monomer molecular parameters $m/a = 550.77/28 = 20 \text{ g mol}^{-1} \text{\AA}^{-1}$ (for **P4** system), where m and a represent, respectively, the mass and the size of a unit.⁶³ A good fit was also observed when comparing the experimental data obtained by dividing M_W by L , the latter being obtained from R_G (Table 4), with the theoretical ones. Thus, one obtains $M_L = 33 \text{ g mol}^{-1} \text{\AA}^{-1}$ for **P4**, $M_L = 32 \text{ g mol}^{-1} \text{\AA}^{-1}$ for **P2** and $M_L = 22 \text{ g mol}^{-1} \text{\AA}^{-1}$ for **P4'**, whereas the theoretical values are $21 \text{ g mol}^{-1} \text{\AA}^{-1}$ for **P2** and $16 \text{ g mol}^{-1} \text{\AA}^{-1}$ for **P4'**. In the three cases studied, the polymers can be seen as rigid molecular threads with a contour length equal to $R_G \times 12^{1/2}$ (Table 4). The rigid character can be well explained by the molecular structure of the dialdehyde used, which has a rigid, preorganized shape (see above) and by the fact that all samples studied, which have different diamines, displayed the same behaviour. The linear density values agreed well with the formation of molecular threads.

Fig. 20 shows the scattering pattern of a four-week-old **P2** sample at $C = 100 \text{ mM}$. At $T = 20^\circ\text{C}$ one observes a low- q upturn characteristic of the presence of aggregates. Such behaviour fits well with the effect of time observed by DOSY NMR spectroscopy (see above). Furthermore, after heating this solution to 60°C , analysis shows that the low- q aggregates signal is no longer present, thus demonstrating the reversible character of these aggregated species. As seen in Table 4, an increase in temperature was shown to shorten the polymeric assemblies giving smaller M_W and R_G values. Such behaviour indicates the reversibility of those polyimines at the covalent level. The calculated sizes show that the objects formed are oligomers rather than polymers and the calculated gyration radii fit well with the hydrodynamic radii obtained by DOSY

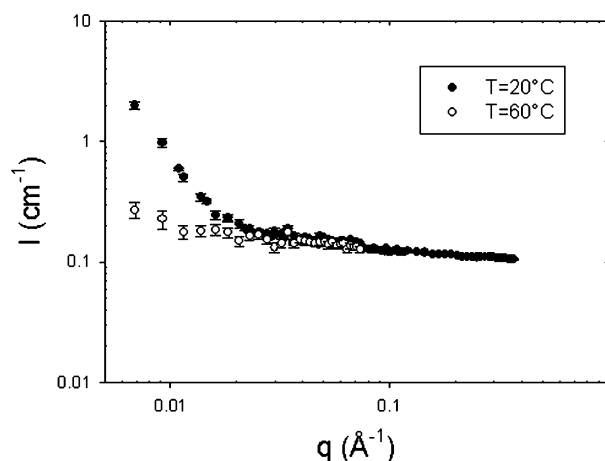


Fig. 20 SANS spectra obtained for an aged, four-week-old **P2** sample at 100 mM .

NMR (see above). Besides the strong temperature effect, the concentration effect was somehow, at first sight, puzzling. In contrast to supramolecular assemblies where an increase in concentration results in an increase in molecular weight,^{61,64} a small decrease in molecular weight was observed when the concentration was increased. According to the theory of polycondensation, the self-assembly of polymers through reversible covalent bonds should give, at the thermodynamic equilibrium, a constant degree of polymerization, independent of the concentration, whose value is related to the equilibrium constant for the formation of the reversible covalent link.^{2,65} The apparent decrease in molecular weight as the concentration is raised might be related to the formation of water in the amine-carbonyl condensation reaction and its state in the chloroform medium. A dehydrated solution, obtained after standing for a few days over anhydrous sodium sulfate, revealed a higher molecular weight (Table 4 and ESI†); the removal of water thus increased the size of the self-assembled species by shifting the reaction towards imine formation.

Combining all those data leads to the conclusion that, with the W-shaped core unit **1**, macrocyclic species are formed at low concentration, whereas oligomeric assemblies are obtained at higher concentration. Such a behaviour was not observed in the case of macrocycles formed from the U-shaped dialdehyde **M-1**, where, from 5 to 50 mM, only the macrocycles **M-1-N₂C₄**, **M-1-N₂C₅**, **M-1-N₂O**, **M-1-N₂O₂** and **M-1-N₂O₃**, were generated, reflecting the fact that the W shape is not as well preorganized to yield macrocyclic species as the U shape is. In the case of the self-assembly between **1-Me** and **N₂O**, ¹H NMR shows one species and MALDI-TOF mass spectrometry identify it as the [2 + 2] macrocycle. However, in the 5–50 mM concentration range, the ¹H NMR spectrum did not change, showing that there was no macrocycle-polymer transition in this case. DOSY NMR data agreed by revealing species of 12.6 Å diameter ($D = 6.40 \times 10^{-10} \text{ m}^2 \text{s}^{-1}$) at 5 mM concentration and a very similar diameter of 13.4 Å ($D = 6.00 \times 10^{-10} \text{ m}^2 \text{s}^{-1}$) at 50 mM concentration in CDCl₃ (ESI†). This peculiar behaviour may be due to a specially stabilized conformation or imine configuration of this macrocycle **1₂-(N₂O)₂**. The presence of four different

imine peaks in the ^1H NMR spectrum indicates indeed a non-symmetric form.

The U-shaped core ligand **2** can also be converted, by addition of metal ions as described above, to W-shaped complexes, which have, in principle, the ability to form polymeric assemblies upon reaction with diamines. As addition of an amine (diamine or monoamine) to **M-2** showed, by ^1H NMR spectroscopy, only partial imine formation, such systems were not studied further since low imine formation would result in a very low degree of polymerization (if polymers were ever formed). On the other hand, the complex **M-2** underwent complete imine formation so that reaction with a diamine could, in principle, form cross-linked metallo-polymers where the cross-linking points are the metal ions. Different diamines (N_2C_4 , N_2C_5 , N_2O , N_2O_2 and N_2O_3) were tried, but in all cases a precipitate was formed. Different solvents and mixture of solvents were tried (CDCl_3 , CD_3NO_2 , CD_3CN , *d*-toluene, CD_3OD , 1,2-dichlorobenzene and their mixtures) but no suitable solvent was found. However, the reaction was complete as ^1H NMR showed no unreacted aldehyde peak after addition of one equiv. of diamine. The insolubility of the self-assembly obtained from **Zn-2** and N_2C_5 together with the fact that no macrocyclic species were observed by MALDI-TOF analysis suggest that it is a cross-linked metallo-polymer. In line with these data, using the diamine $\text{N}_2\text{C}_3'$, soluble assemblies with **Zn-2** were obtained, whose polymeric nature was indicated by DOSY NMR spectroscopy. At 5 mM concentration in CDCl_3 - CD_3CN (6 : 4), small objects of 19 Å diameter ($D = 460 \mu\text{m}^2 \text{s}^{-1}$) were observed, whereas at 50 mM concentration, much larger ones of 62 Å diameter ($D = 140 \mu\text{m}^2 \text{s}^{-1}$) were found (ESI†). In the metal-free state, the reaction between $\text{N}_2\text{C}_3'$ and **2** afforded the corresponding [2 + 2] macrocycle as in the case of N_2C_3 described above (Fig. 21).

Constitutional switching in response to shape changes. The results described above show that core units of different shapes, W and U, yield products of different constitution when undergoing covalent self-assembly processes. Since

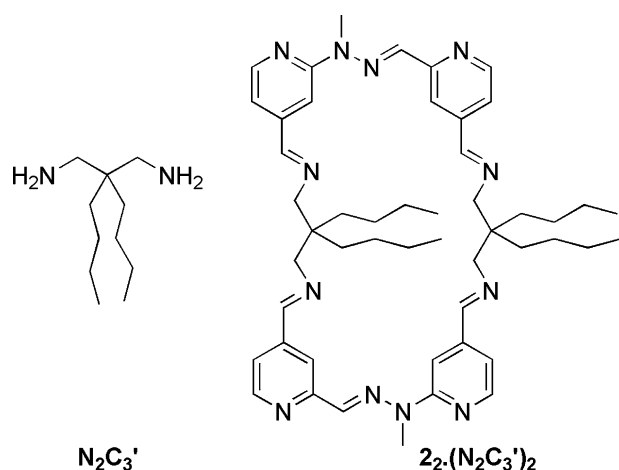
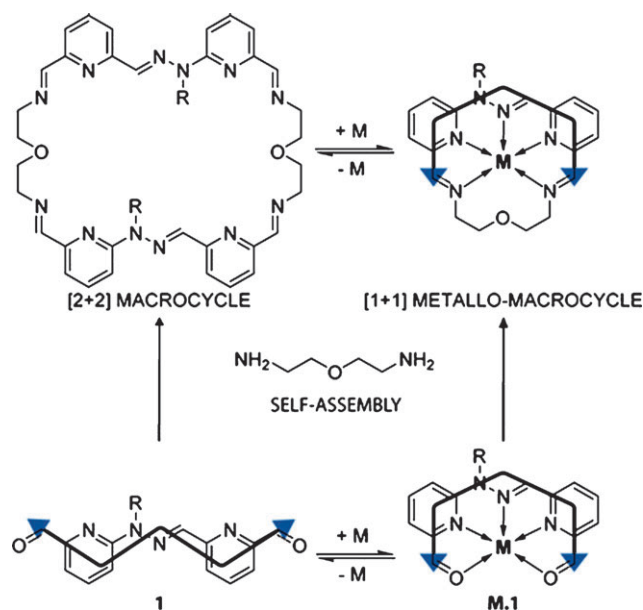


Fig. 21 Molecular structure of $\text{N}_2\text{C}_3'$ and its [2 + 2] macrocycle $22 \cdot (\text{N}_2\text{C}_3')_2$ formed by condensation with **2**. The [2 + 2] macrocycle is expected to be a mixture of *syn* and *anti* products with respect to the relative position of the hydrazone.

the shape of these morphological switches can be changed reversibly, it should be possible to switch reversibly the constitution of the species formed, between two states by simply changing the shape state of the morphological switch present. Such constitutional switching between macrocycles and polymers is depicted in Scheme 1. It may face practical difficulties, as ideally the different species formed should be soluble in the same medium and at relatively high concentration (typically 50 mM to favour polymeric species rather than macrocyclic ones in the W-shaped state).

Macrocycle–macrocycle interconversion. To probe the feasibility of such constitutional interconversion, a more simple case, the conversion between two different types of macrocycle (Scheme 5), was first tested. As described above, the self-assembly between **1-Me** and N_2O resulted in the selective formation of the corresponding [2 + 2] macrocycle whereas the corresponding [1 + 1] metallo-macrocycle **Zn-1-Me-N2O** was obtained with the complexed U-shaped core. It should therefore be possible to reversibly interconvert the constitutionally different states by reversible shape-switching on metal ion binding or release.

^1H NMR spectroscopy was used to monitor the conversion of one species into the other one. The addition of zinc triflate to the [2 + 2] macrocycle $12 \cdot (\text{N}_2\text{O})_2$ showed the immediate conversion into the [1 + 1] metallo-macrocycle **Zn-1-N2O** (ESI†), indicating that constitutional conversion indeed occurs on shape change triggered by addition of a metal ion. Removal of the metal ion by addition of hexacyclen causes reversion to the [2 + 2] species, although it required a longer time (ESI†).



Scheme 5 Schematic representation of the principle of constitutional switches between two different kinds of macrocycles, namely a [2 + 2] and a [1 + 1] macrocycle, in response to W–U shape change. Note that the [2 + 2] macrocycles is expected to be a mixture of *syn* and *anti* products with respect to the relative position of the hydrazone; the *anti* product is depicted here.

Although in the case of the diamine N_2C_5 at 5 mM, the [2 + 2] macrocycle is not fully formed, addition of the metal salt drives the system nevertheless to full conversion into the [1 + 1] macrocycle complex $\text{M}\cdot\text{1-N}_2\text{C}_5$.

Polymer–macrocycle interconversion. The polymers made by self-assembly with **1-Me** are soluble in chloroform solutions but addition of acetonitrile induces precipitation. On the other hand, acetonitrile is required to solubilize the corresponding metal complexes. The ligand **1-Oct** proved to be much more tolerant to the presence of acetonitrile. A constitutional switching process could then be performed in the appropriate solvent over a few hours by sequences of addition of metal ions and their removal by addition of a better binder, hexacyclen in the case of Zn(II) and cryptand [2.2.2] in the case of Pb(II) (Fig. 22). Except in the case between **P2** and **Zn-1-Oct-N₂C₅**, no fatigue in constitutional change was observed after 4–6 interconversions.

The second system tested involved the *in situ* conversion between a cross-linked metallo-polymer and an organic macrocycle. Such conversion could be achieved with **Zn-2₂** and N_2C_5 even though the cross-linked polymer was an insoluble material (as discussed above). Addition of 0.5 equiv. of hexacyclen to the heterogeneous systems containing the cross-linked metallo-polymer resulted in complete

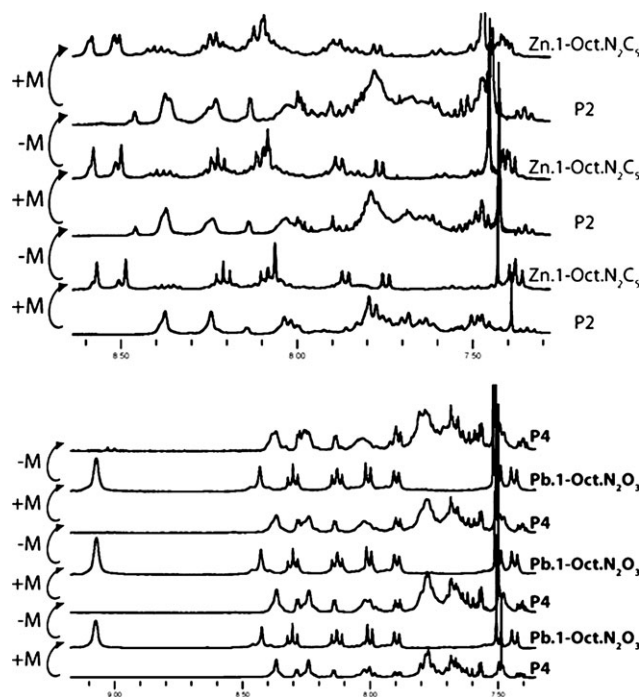


Fig. 22 ^1H NMR spectra showing the reversible constitutional conversion between polyimine polymers and metallo-macrocycles at 50 mM of each starting material. *Top*: between **P2** and **Zn-1-Oct-N₂C₅** in $\text{CDCl}_3\text{-CD}_3\text{CN}$ (8 : 2). *Bottom*: between **P4** and **Pb-1-Oct-N₂O₃** in $\text{CDCl}_3\text{-CD}_3\text{CN}$ (6 : 4). “+M” refers to the addition of 1.0 equiv. of the metal salt, either zinc triflate or lead triflate, and “-M” refers to the addition of 1.0 equiv. of, respectively, either hexacyclen or cryptand [2.2.2]. The high concentration used ensures complete interconversion.

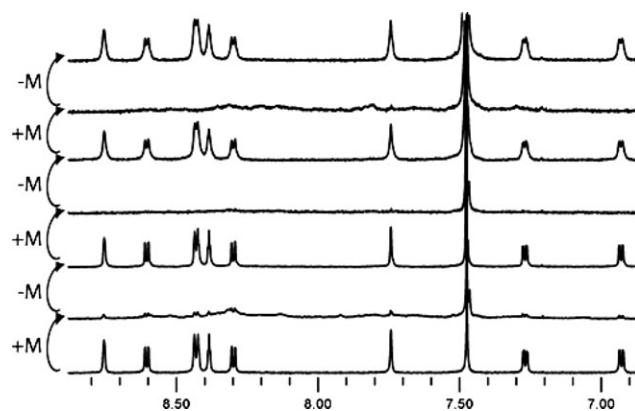


Fig. 23 ^1H NMR spectra showing the reversible constitutional conversion between insoluble cross-linked metallo-polymer made from **Zn-2₂** and N_2C_5 and organic [1 + 1] macrocycle **2-N₂C₅** at 5 mM of each starting material in $\text{CDCl}_3\text{-CD}_3\text{CN}$ (6 : 4). “+M” refers to the addition of 0.5 equiv. of zinc triflate and “-M” refers to the addition of 0.5 equiv. of hexacyclen.

solubilization of the material and formation of the organic macrocycle **2-N₂C₅** after imine swapping. Subsequent addition of 0.5 equiv. of zinc triflate reverted the system to the cross-linked polymer, which then precipitated out from the solution (Fig. 23).

Such a process operating with a phase change has recently been shown to be useful in terms of producing mechanical energy.⁶⁶ The use of the branched diamine $\text{N}_2\text{C}_3'$ gave a soluble polymer. The reversible conversion between the [2 + 2] macrocycle **2₂-(N₂C₃')₂** and the cross-linked metallo-polymer made from **Zn-2₂** and $\text{N}_2\text{C}_3'$ could then be achieved in the solution state, as demonstrated by ^1H NMR spectroscopy and illustrated in Fig. 24.

In summary, morphological switches controlled by metal ions allowed the whole system to reversibly switch between two different constitutional states.

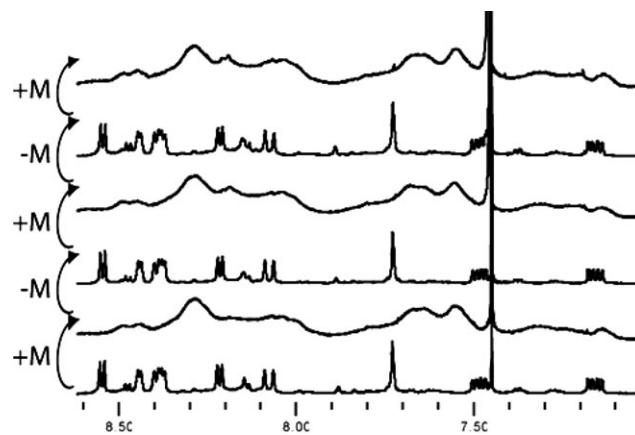


Fig. 24 ^1H NMR spectra showing the reversible constitutional conversion between the cross-linked metallo-polymer made from **Zn-2₂** and $\text{N}_2\text{C}_3'$ and the organic [2 + 2] macrocycle **2₂-(N₂C₃')₂** at 50 mM of each starting material in $\text{CDCl}_3\text{-CD}_3\text{CN}$ (6 : 4). “+M” refers to the addition of 0.5 equiv. of zinc triflate and “-M” refers to the addition of 0.5 equiv. of hexacyclen.

Conclusion

The results reported here describe the design, synthesis and operation of two different morphological switches, whose shape states are controlled by metal ions. Such switches were appended with aldehyde groups in order to connect them covalently but reversibly to different constitutional states through imine formation. The well-defined W and U shapes were shown to induce the formation of a particular type of object. U-shaped molecules induced the formation of macrocycles through imine condensation. On the other hand, W-shaped molecules yielded macrocyclic species at low concentration whereas an increase in concentration resulted in a constitutional change in favour of linear polymeric species.

The present work demonstrates that a particular molecular shape can be directly translated into a specific constitution through covalent self-assembly. The shape change induced the whole dynamic system to change its constitution through covalent bond rearrangement in order to relax the structural perturbation that it causes. Constitutional switching between polymeric and macrocyclic species was achieved quantitatively over a few interconversion cycles. The processes described involve the translation of structural information of a morphological switch into well-defined constitutional states that are directly correlated to the shape state of the switch. They demonstrate the ability of constitutional dynamic systems to undergo adaptation to morphological changes through constitutional variation.

Experimental

General

All reagents were purchased from commercial suppliers and used without further purification unless otherwise noted. The diamine N_2C_3' was synthesized as previously described.⁶⁷ Anhydrous DMF was bought from the Aldrich company. Technical DCM was bought with amylene as stabilizer. DCM was dried either over phosphorus pentachloride or by passing through a column of activated alumina and copper oxide. THF was dried either over sodium in the presence of benzophenone or by passing through a column of activated alumina and copper oxide. Metal salts were dried by gentle heating at 60 °C under vacuum for a few hours. $CDCl_3^*$ denotes the use of $CDCl_3$ that was filtered through basic alumina to remove traces of acidity. Flash column chromatography was performed using silica gel (Si 60, 40–63 μ m, Merck) or neutral alumina (Aluminium oxide 90 active neutral, Activity stage I, Merck) on a classical glass column or with a FlashPack system using prepacked columns when noted.

1H NMR spectra were recorded on a Bruker Avance 400 spectrometer at 400 MHz. Chemical shifts are given in ppm. Residual solvent peaks were taken as reference ($CDCl_3$: 7.26 ppm, CD_3CN : 1.94 ppm, CD_3OD : 3.31 ppm).⁶⁸ The coupling constants J are given in Hz. Peaks are described as singlet (s), doublet (d), triplet (t), doublet of doublet (dd), multiplet (m) and broad (br). The assigned proton is written in italic. Unless otherwise noted, spectra were recorded at 25 °C. When noted, spectra were recorded on a 500 MHz Bruker

Avance 500 spectrometer at 500 MHz. ^{13}C NMR spectra were recorded on a Bruker Avance 400 spectrometer at 100 MHz. All spectra were measured under broadband decoupled conditions. Chemical shifts are given in ppm. Residual solvent peak were taken as reference ($CDCl_3$: 77.0 ppm, CD_3CN : 1.24 ppm, CD_3OD : 49.05 ppm).⁶⁸ When mixtures of solvent were used, the calibration was done using the residual solvent peak of CD_3CN in the case of $CDCl_3$ – CD_3CN mixtures and CD_3OD in the case of $CDCl_3$ – CD_3OD mixtures. 2D NMR (COSY, ROESY, HSQC, HMBC) were recorded either on a Bruker Avance 400 spectrometer or, when noted, on a 500 MHz Bruker Avance 500 spectrometer. Diffusion-ordered spectroscopy (DOSY) measurements were performed on a Bruker Avance 500 spectrometer. The values of viscosity for $CDCl_3$ – CD_3CN mixtures were obtained from the literature.⁶⁹

High resolution electrospray ionization mass spectrometry (HR-ESI-MS) analyses were performed on a Bruker Micro TOF mass spectrometer at the Service de Spectrométrie de Masse, Université Louis Pasteur. The given value represents the largest peak. The observed pattern was always conformed to the theoretical pattern. MALDI-TOF analyses were performed on a Bruker AutoFlex II mass spectrometer at the Service de Spectrométrie de Masse, Université Louis Pasteur. The given value represents the largest peak. The observed pattern was always conformed to the theoretical pattern. Direct analysis of solid was performed by MALDI-TOF analyses on a Bruker AutoFlex II (Laser N₂, λ = 337 nm, frequency 1 Hz) at a 90 ms pulsed ion extraction and a 20 kV reflectron using the positive mode detection. Calibration was performed by using a mixture of standard peptides. The given value represents the largest peak. The observed pattern was always conformed to the theoretical pattern. The sample was prepared by grinding *ca.* 1 mg of product with *ca.* 10 mg of matrix in a mortar. The homogeneous solid mixture was deposited on a conductive tape (Ref. 9703, 3M, Radiospares) and analysis was performed. Electronic absorption spectroscopy was performed on a Varian CARY 3 spectrophotometer in the UV-visible range.

X-Ray structure determinations

The X-ray crystallographic structural determinations were performed at the Service de Radiocristallographie, Université Louis Pasteur. The crystals were placed in oil and a single crystal was selected, mounted on a glass fibre and placed in a low-temperature nitrogen stream. The X-ray diffraction data were collected on a Nonius-Kappa-CCD diffractometer with a graphite monochromatized Mo-K α radiation (λ = 0.71073 Å), phi scans, by using a “phi-scan” type scan mode. Crystal structures of **1-Me**, **Zn-1-Me-N₂C₄**, **Zn-1-Me-N₂C₅**, **2₂(N₂C₃)₂**, **4-H**, **4-Me**, **Pb-1-Me**, **Pb-1-Me-N₂O₂**, **Pb-2** and **Zn-1-Me** were deposited at CCDC under the reference numbers 703869, 703870, 703871, 703872, 703873, 703874, 703875, 703876, respectively.

Small-angle neutron scattering experiments

Small-angle neutron scattering experiments were carried out on the PACE spectrometer in Léon Brillouin laboratory, Saclay. The chosen incident wavelength, λ , depends on the set of experiments, as follows. For a given wavelength, the

range of the amplitude of the transfer wave vector, q , was selected by changing the detector distance, D_d . Three sets of sample-to-detector distances and wavelength were chosen ($D_d = 0.86$ m, $\lambda = 6 \pm 0.5$ Å; $D_d = 3$ m, $\lambda = 6 \pm 0.5$ Å; and $D_d = 4.7$ m, $\lambda = 6 \pm 0.5$ Å) so that the following q -ranges were, respectively, available: $3.63 \times 10^{-2} \leq q$ (Å⁻¹) $\leq 3.69 \times 10^{-1}$, $1.1 \times 10^{-2} \leq q$ (Å⁻¹) $\leq 1.165 \times 10^{-1}$, and $6.88 \times 10^{-3} \leq q$ (Å⁻¹) $\leq 7.32 \times 10^{-2}$. Measured intensities were calibrated to absolute values (cm⁻¹) using normalization by the attenuated direct beam classical method. Standard procedures to correct the data for the transmission, detector efficiency and backgrounds (solvent, empty cell, electronic and neutronic background) were carried out. The scattered wave vector, q , is defined by eqn (3), where θ is the scattering angle:

$$q = \frac{4\pi}{\lambda} \sin \frac{\theta}{2} \quad (3)$$

§ X-Ray crystallographic data for **2₂·(N₂C₃)₂**: [C₃₇H₃₆N_{13.50}]; 669.79 g mol⁻¹; monoclinic; space group C2; $a = 26.46(2)$, $b = 4.493(4)$, $c = 17.260(13)$ Å; $\alpha = 90.00$, $\beta = 111.24(4)$, $\gamma = 90.00^\circ$; $V = 1912(3)$ Å³; density: 1.163 g cm⁻³; $T = 273(2)$ K; $Z = 2$; $F(000)$: 705; number of data measured: 3793; number of data with $I > 2\sigma(I)$: 1962; number of variables: 420; $R = 0.0898$; $R_w = 0.2179$; goodness-of-fit = 0.969. X-Ray crystallographic data for **4-H**: [C₁₉H₂₈N₄O₂Si]; 372.54 g mol⁻¹; monoclinic; space group $P2_1/n$; $a = 6.4521(2)$, $b = 28.5690(13)$, $c = 11.0892(4)$ Å; $\alpha = 90.00$, $\beta = 92.813(2)$, $\gamma = 90.00^\circ$; $V = 2041.61(13)$ Å³; density: 1.212 g cm⁻³; $T = 173(2)$ K; $Z = 4$; $F(000)$: 800; number of data measured: 4669; number of data with $I > 2\sigma(I)$: 2580; number of variables: 241; $R = 0.0540$; $R_w = 0.1133$; goodness-of-fit = 1.000. X-Ray crystallographic data for **4-Me**: [C₂₀H₃₀N₄O₂Si]; 386.57 g mol⁻¹; triclinic; space group $P\bar{1}$; $a = 7.2195(4)$, $b = 11.2353(4)$, $c = 13.5800(6)$ Å; $\alpha = 92.830(3)$, $\beta = 102.655(2)$, $\gamma = 92.846(3)^\circ$; $V = 1071.38(8)$ Å³; density: 1.198 g cm⁻³; $T = 293(2)$ K; $Z = 2$; $F(000)$: 416; number of data measured: 4895; number of data with $I > 2\sigma(I)$: 3296; number of variables: 319; $R = 0.0528$; $R_w = 0.1337$; goodness-of-fit = 1.039. X-Ray crystallographic data for **Pb-1-Me**: [C₃₂H₂₄F₁₂N₈O₁₆Pb₂S₄]; 1547.22 g mol⁻¹; monoclinic; space group $P2_1/c$; $a = 10.2401(3)$, $b = 13.1113(6)$, $c = 17.6193(7)$ Å; $\alpha = 90.00$, $\beta = 98.972(2)$, $\gamma = 90.00^\circ$; $V = 2336.64(16)$ Å³; density: 2.199 g cm⁻³; $T = 173(2)$ K; $Z = 2$; $F(000)$: 1472; number of data measured: 5341; number of data with $I > 2\sigma(I)$: 4032; number of variables: 335; $R = 0.0338$; $R_w = 0.0699$; goodness-of-fit = 1.014. X-Ray crystallographic data for **Pb-1-Me·N₂O₂**: [C₂₂H₂₄F₆N₆O₈PbS₂]; 885.78 g mol⁻¹; monoclinic; space group $P2_1/c$; $a = 8.7467(2)$, $b = 13.0859(5)$, $c = 26.4906(8)$ Å; $\alpha = 90.00$, $\beta = 97.775(2)$, $\gamma = 90.00^\circ$; $V = 3004.20(16)$ Å³; density: 1.958 g cm⁻³; $T = 173(2)$ K; $Z = 4$; $F(000)$: 1720; number of data measured: 6841; number of data with $I > 2\sigma(I)$: 4398; number of variables: 407; $R = 0.0620$; $R_w = 0.1292$; goodness-of-fit = 1.038. X-Ray crystallographic data for **Pb-2**: [C₁₆H₁₂F₆N₄O₈PbS₂]; 773.61 g mol⁻¹; monoclinic; space group $P2_1/n$; $a = 9.5365(19)$, $b = 12.446(3)$, $c = 10.605(2)$ Å; $\alpha = 90.00$, $\beta = 110.52(3)$, $\gamma = 90.00^\circ$; $V = 1178.9(4)$ Å³; density: 2.179 g cm⁻³; $T = 173(2)$ K; $Z = 2$; $F(000)$: 736; number of data measured: 2709; number of data with $I > 2\sigma(I)$: 2281; number of variables: 174; $R = 0.0429$; $R_w = 0.1041$; goodness-of-fit = 1.064. X-Ray crystallographic data for **Zn-1-Me**: [C₁₆H₁₂F₆N₄O₈S₂Zn]; 631.79 g mol⁻¹; monoclinic; space group $C2/c$; $a = 11.6632(15)$, $b = 22.296(4)$, $c = 8.5280(8)$ Å; $\alpha = 90.00$, $\beta = 93.860(8)$, $\gamma = 90.00^\circ$; $V = 2212.6(5)$ Å³; density: 1.897 g cm⁻³; $T = 173(2)$ K; $Z = 4$; $F(000)$: 1264; number of data measured: 2511; number of data with $I > 2\sigma(I)$: 1541; number of variables: 174; $R = 0.1171$; $R_w = 0.1503$; goodness-of-fit = 1.223. X-Ray crystallographic data for **Zn-1-Me·N₂C₅**: [C₂₁H₂₄F₆N₆O₇S₂Zn]; 715.95 g mol⁻¹; Orthorhombic; space group $Pna2_1$; $a = 25.1170(4)$, $b = 11.8990(6)$, $c = 9.3020(12)$ Å; $\alpha = 90.00$, $\beta = 90.00$, $\gamma = 90.00^\circ$; $V = 2780.1(4)$ Å³; density: 1.711 g cm⁻³; $T = 173(2)$ K; $Z = 4$; $F(000)$: 1456; number of data measured: 7069; number of data with $I > 2\sigma(I)$: 3630; number of variables: 397; $R = 0.0680$; $R_w = 0.1108$; goodness-of-fit = 1.006.

The usual equation for absolute neutron scattering combines the intraparticle scattering $S_1(q) = V_{\text{chain}}\phi_{\text{vol}}P(q)$ form factor with the interparticle scattering $S_2(q)$ factor:

$$I(q)(\text{cm}^{-1}) = (\Delta\rho)^2(S_1(q) + S_2(q)) \\ = (\Delta\rho)^2(V_{\text{chain}}\phi_{\text{vol}}P(q) + S_2(q)) \quad (4)$$

where $(\Delta\rho)^2 = (\rho_{\text{monomer}} - \rho_{\text{solvent}})^2$ is a contrast per unit volume between the polymer and the solvent and was determined from the known chemical composition. $\rho = \sum_i b_i/(\sum_i m_i v \times 1.66 \times 10^{-24})$ represents the scattering length per unit volume, b_i is the neutron scattering length of the species i , m_i the mass of species i , and v the specific volume of the monomer (which has been measured, the values being equal to 0.89 (**P4**), 0.874 (**P2**), and 0.815 (for **P4'**) cm³ g⁻¹) or the solvent (*i.e.*, 0.67 cm³ g⁻¹ for CDCl₃). $P(q)$ is the form factor, $V_{\text{chain}} = Nvm \times 1.66 \times 10^{-24}$ is the volume of the N monomers (of mass m) in a chain and ϕ_{vol} is the volume fraction of monomer. In the high q -range, the scattering is assumed to arise from isolated chains; *i.e.*, $S_2(q) = 0$, and thus $I(q) \propto P(q)$.

Elemental analyses were performed at the Service de Micro-analyse, Université Louis Pasteur. Data are given in percentage. Kinetic studies were performed using 400 MHz ¹H NMR spectroscopy. The sample spinning was set to 20 Hz.

Syntheses

(6-(1-Methylhydrazinyl)pyridin-2-yl)methanol 6-Me. Methylhydrazine (80 mL) was added to (6-bromopyridin-2-yl)methanol (1.74 g, 9.25 mmol) and the mixture was heated at reflux under a nitrogen atmosphere overnight. The reaction mixture was then concentrated *in vacuo*. The residue was dissolved in CHCl₃, and K₂CO₃ was added. The mixture was filtered and concentrated *in vacuo*. This quantitative crude product was directly used in the next step. ¹H NMR (CDCl₃): 7.34 (t, $J = 7.5$, 1H), 6.68 (d, $J = 8.3$, 1H), 7.52 (d, $J = 6.5$, 1H), 4.49 (br, 2H, CH₂), 4.18 (br, 3H), 3.12 (s, 3H, CH₃); ¹³C NMR (CDCl₃): 160.1, 156.7, 137.5, 108.5, 105.1, 63.8, 40.5.

(6-Hydrazinylpyridin-2-yl)methanol 6-H. Hydrazine monohydrate (70 mL) was added to (6-bromopyridin-2-yl)methanol (1.50 g, 7.98 mmol) and the mixture was heated at 130 °C under a nitrogen atmosphere overnight. The reaction mixture was then concentrated *in vacuo*. The residue was dissolved in CHCl₃, and K₂CO₃ was added. The mixture was filtered and concentrated *in vacuo*. This quantitative crude product was directly used in the next step. ¹H NMR (CDCl₃): 7.48 (t, $J = 8.0$, 1H), 6.60 (d, $J = 8.0$, 2H), 6.18 (br, 1H), 4.60 (s, 2H), 3.95 (br, 3H); ESI-MS: calculated for [C₆H₉N₃O + H]⁺ 140.0818, found 140.2437.

6-(Hydroxymethyl)pyridine-2-carbaldehyde 7. The product was prepared using a modified literature procedure.⁷⁰ 2,6-Pyridinedimethanol (9.96 g, 71.56 mmol) was dissolved in CHCl₃ (1 L). Manganese dioxide (6.22 g, 71.56 mmol) was then added and the mixture was stirred at room temperature under nitrogen atmosphere. After every 2–3 days, 0.2 equiv. of manganese dioxide were added. The reaction was monitored by TLC until no further conversion was observed upon addition of manganese dioxide. The reaction mixture was then

filtered through celite and purified by flash chromatography on silica (eluent: DCM \rightarrow 2% MeOH). The resulting oily product was dried under vacuum for 24 hours to give 6.27 g (64%) of a beige solid. ^1H NMR (CDCl_3): 10.07 (s, 1H, CHO), 7.88 (m, 2H), 7.52 (m, 1H), 4.87 (s, 2H, CH_2); ^{13}C NMR (CDCl_3): 193.0 (CHO), 160.1, 151.6, 137.7, 124.8, 120.5, 64.1 (CH_2); HR-ESI-MS: calculated for $[\text{C}_7\text{H}_7\text{NO}_2 + \text{Li}]^+$ 144.0637, found 144.0653, $[\text{C}_7\text{H}_7\text{NO}_2 + \text{Na}]^+$ 160.0374, found 160.0407; elemental analysis: calculated for $[\text{C}_7\text{H}_7\text{NO}_2]$ C 61.31, H 5.14, N 10.21, found C 61.34, H 5.41, N 10.23.

(E)-6-((2-(6-(Hydroxymethyl)pyridin-2-yl)-2-methylhydrazono)-methyl)pyridin-2-yl)methanol 3-Me. (6-(1-Methylhydrazinyl)pyridin-2-yl)methanol **6-Me** (1.42 g, 9.25 mmol) was dissolved in CHCl_3 (250 mL). 6-(Hydroxymethyl)pyridine-2-carbaldehyde **7** (1.27 g, 9.25 mmol) was added and the reaction mixture was stirred for 2 days at room temperature under a nitrogen atmosphere. The reaction mixture was then concentrated *in vacuo*. Recrystallization in Et_2O afford 2.11 g (84%) of a pale yellow solid. ^1H NMR (CD_3OD): 7.96 (d, $J = 7.8$, 1H), 7.84 (t, $J = 7.8$, 1H), 7.76 (s, 1H), 7.67 (m, 2H), 7.43 (d, $J = 7.3$, 1H), 6.99 (d, $J = 6.9$, 1H), 4.71 (s, 2H), 4.61 (s, 2H), 3.70 (s, 3H, NCH_3); ^{13}C NMR (CD_3OD): 161.9, 159.9, 158.2, 156.0, 139.5, 138.9, 134.8, 120.7, 119.1, 113.8, 109.5, 66.1, 65.6, 30.0; HR-ESI-MS: calculated for $[\text{C}_{14}\text{H}_{16}\text{N}_4\text{O}_2 + \text{H}]^+$ 273.1352, found 273.1351; elemental analysis: calculated for $[\text{C}_{14}\text{H}_{16}\text{N}_4\text{O}_2]$ C 61.75, H 5.92, N 20.58, found C 61.32, H 5.904, N 20.76.

(E)-6-((2-(6-(Hydroxymethyl)pyridin-2-yl)hydrazono)methyl)pyridin-2-yl)methanol 3-H. (6-Hydrazinylpyridin-2-yl)methanol **6-H** (1.11 g, 7.98 mmol) was dissolved in CHCl_3 (200 mL). 6-(Hydroxymethyl)pyridine-2-carbaldehyde **7** (1.09 g, 7.98 mmol) was added and the reaction mixture was stirred for 3–4 days at room temperature under a nitrogen atmosphere. The reaction mixture was then concentrated *in vacuo*. Recrystallization in Et_2O afford 1.73 g (84%) of a pale beige solid. ^1H NMR (CD_3OD): 7.96 (s, 1H), 7.94 (d, $J = 8.4$, 1H), 7.83 (t, $J = 7.8$, 1H), 7.68 (t, $J = 7.6$, 1H), 7.45 (d, $J = 7.6$, 1H), 7.24 (d, $J = 8.0$, 1H), 6.95 (d, $J = 7.2$, 1H), 4.70 (s, 2H), 4.57 (s, 2H); ^{13}C NMR (CD_3OD): 162.0, 160.6, 157.6, 155.2, 140.0, 139.7, 138.8, 121.0, 119.5, 113.4, 107.1, 65.6, 65.5; HR-ESI-MS: calculated for $[\text{C}_{13}\text{H}_{14}\text{N}_4\text{O}_2 + \text{Na}]^+$ 281.1014, found 281.0967.

(E)-6-((2-(6-(Hydroxymethyl)pyridin-2-yl)-2-octylhydrazono)-methyl)pyridin-2-yl)methanol 3-Oct. Sodium hydride (60% w/w oil dispersion, 320 mg, 7.68 mmol) was suspended in 15 mL of anhydrous DMF. **3-H** (400 mg, 1.55 mmole) was added and the reaction mixture was stirred at room temperature under a nitrogen atmosphere for 1 hour. 1-Bromooctane (267 μL , 1.55 mmol) was slowly added to the red–brown mixture. After 3 hours, DCM and brine were added. The organic layer was dried over sodium sulfate and concentrated *in vacuo*. Purification by flash chromatography on neutral alumina, deactivated with 5% water (eluent: DCM \rightarrow 1% MeOH), gave 400 mg (70%) of a white-yellow solid. ^1H NMR (CDCl_3^*): 7.91 (d, $J = 7.6$, 1H), 7.77 (s, 1H), 7.70 (t, $J = 7.6$, 1H), 7.59 (m, 2H), 7.14 (d, $J = 7.6$, 1H), 6.74 (m, 1H), 4.78 (s, 2H), 4.69 (s, 2H), 4.31 (t, $J = 8.0$, 2H), 3.79 (br, 1H), 3.66 (br, 1H), 1.70 (m, 2H), 1.35 (m, 10H), 0.87 (t, $J = 6.8$, 3H); ^{13}C NMR (CDCl_3^*): 158.3,

156.5, 156.4, 154.3, 138.2, 136.9, 134.0, 119.1, 117.8, 112.0, 108.3, 64.0, 63.8, 42.2, 31.8, 29.4, 29.2, 27.2, 24.9, 22.6, 14.1; HR-ESI-MS: calculated for $[\text{C}_{21}\text{H}_{30}\text{N}_4\text{O}_2 + \text{Na}]^+$ 393.2266, found 393.2288.

(E)-6-((2-(6-Formylpyridin-2-yl)-2-methylhydrazono)methyl)-picolinaldehyde 1-Me. 3-Me (50 mg, 0.184 mmol) and Dess–Martin periodinane (187 mg, 0.441 mmol) were placed in a flask under a nitrogen atmosphere. Anhydrous DCM (10 mL) was added and the mixture was stirred at room temperature for 4 hours. A saturated solution of NaHCO_3 and $\text{Na}_2\text{S}_2\text{O}_3$ (766 mg) were then added and the heterogeneous solution was stirred vigorously overnight. The organic layer was washed twice with a saturated solution of NaHCO_3 and the aqueous layer was back extracted with DCM. The organic layers were combined, dried over sodium sulfate and concentrated *in vacuo* to give a quantitative light yellow solid. ^1H NMR (CDCl_3^*): 10.09 (s, 1H), 9.99 (s, 1H), 8.24 (dd, $J = 7.3$, $J = 1.5$, 1H), 7.98 (d, $J = 8.3$, 1H), 7.90 (m, 3H), 7.80 (t, $J = 8.3$, 1H), 7.53 (d, $J = 7.8$, 1H), 3.82 (s, 3H); ^1H NMR (500 MHz, $\text{CDCl}_3^*-\text{CD}_3\text{CN}$ (6 : 4)): 10.03 (d, $J = 1.0$, 1H, H_3), 9.94 (d, $J = 1.0$, 1H, H_{10}), 8.26 (dd, $J = 8.0$, $J = 1.0$, 1H, H_6), 8.01 (dd, $J = 8.5$, $J = 1.0$, 1H, H_7), 7.94 (t, $J = 7.5$, 1H, H_5), 7.88 (s, 1H, H_2), 7.83 (m, 2H, H_8 and H_4), 7.48 (dd, $J = 7.0$, $J = 1.0$, 1H, H_9), 3.79 (d, $J = 1.0$, 3H, H_1); ^{13}C NMR (CDCl_3^*): 193.4, 193.1 (CH_3), 157.4, 155.7 (CCH_6), 152.4 (CCH_3), 150.5 (CCH_{10}), 138.4, 137.3 (CH_5), 134.7 (CH_2), 123.5 (CH_6), 121.0, 114.8, 114.7, 29.8 (CH_1); HR-ESI-MS: calculated for $[\text{C}_{14}\text{H}_{12}\text{N}_4\text{O}_2 + \text{Li}]^+$ 275.1120, found 275.1126, $[\text{C}_{14}\text{H}_{12}\text{N}_4\text{O}_2 + \text{Na}]^+$ 291.0858, found 291.0863, $[\text{C}_{14}\text{H}_{12}\text{N}_4\text{O}_2 + \text{K}]^+$ 307.0597, found 307.0617.

(E)-6-((2-(6-Formylpyridin-2-yl)-2-octylhydrazono)methyl)-picolinaldehyde 1-Oct. 3-Oct (30 mg, 0.081 mmol) and Dess–Martin periodinane (82 mg, 0.194 mmol) were placed in a flask under a nitrogen atmosphere. Anhydrous DCM (4.4 mL) was added and the mixture was stirred at room temperature for 4 hours. A saturated aqueous solution of NaHCO_3 and $\text{Na}_2\text{S}_2\text{O}_3$ (341 mg) were then added and the heterogeneous solution was stirred vigorously overnight. The organic layer was washed twice with a saturated aqueous solution of NaHCO_3 , dried over sodium sulfate and concentrated *in vacuo* to give a quantitative light yellow solid. ^1H NMR (CDCl_3^*): 10.08 (s, 1H), 9.95 (s, 1H), 8.21 (dd, $J = 7.6$, $J = 1.6$, 1H), 7.88 (m, 4H), 7.76 (t, $J = 8.0$, 1H), 7.50 (dd, $J = 7.2$, $J = 0.8$, 1H), 4.42 (t, $J = 7.2$, 2H, NCH_2), 1.72 (m, 2H), 1.35 (m, 10H), 0.85 (t, $J = 6.8$, 3H); ^{13}C NMR (CDCl_3^*): 193.5, 193.0, 157.2, 155.9, 152.3, 150.5, 138.2, 137.1, 133.8, 123.4, 121.0, 114.5, 114.3, 42.1, 31.7, 29.2, 29.1, 26.9, 24.7, 22.6, 14.0; HR-ESI-MS: calculated for $[\text{C}_{21}\text{H}_{26}\text{N}_4\text{O}_2 + \text{Li}]^+$ 373.2216, found 373.2229, $[\text{C}_{21}\text{H}_{26}\text{N}_4\text{O}_2 + \text{Na}]^+$ 389.1953, found 389.1970.

(2-(1-Methylhydrazinyl)pyridin-4-yl)methanol 8-Me. Methylhydrazine (16 mL) was added to (2-bromopyridin-4-yl)methanol (292 mg, 1.55 mmol) and the reaction mixture was heated at reflux under a nitrogen atmosphere overnight. The reaction mixture was then concentrated *in vacuo*. The residue was dissolved in CHCl_3 , and K_2CO_3 was added. The mixture was filtered and concentrated *in vacuo*. This

quantitative crude product was directly used in the next step. ^1H NMR (CDCl_3): 7.96 (d, $J = 4.9$, 1H), 6.86 (s, 1H), 6.49 (d, $J = 5.4$, 1H), 4.52 (s, 2H), 3.91 (br. s, 3H), 3.16 (s, 3H); ^{13}C NMR (CDCl_3): 161.3, 151.8, 147.0, 110.7, 104.1, 63.3, 40.9.

(2-Hydrazinylpyridin-4-yl)methanol 8-H. Hydrazine monohydrate (50 mL) was added to (2-bromopyridin-4-yl)methanol (1.02 g, 5.42 mmol) and the reaction mixture was heated at 130 °C under a nitrogen atmosphere overnight. The reaction mixture was then concentrated *in vacuo*. The residue was dissolved in CHCl_3 , and K_2CO_3 was added. The mixture was filtered and concentrated *in vacuo*. This quantitative white solid was directly used in the next step. ^1H NMR (CD_3OD): 7.92 (d, $J = 5.2$, 1H), 6.79 (s, 1H), 6.63 (d, $J = 5.6$, 1H), 4.84 (br, 4H), 4.55 (s, 2H, CH_2); ^{13}C NMR (CD_3OD): 162.9, 154.0, 147.5, 112.7, 105.2, 63.7.

4-((tert-Butyldimethylsilyloxy)methyl)picolinaldehyde 9. 2-Bromo-4-((tert-butyldimethylsilyloxy)methyl)pyridine **10** (616 mg, 2.04 mmol) was dissolved in dry THF (12.5 mL) under a nitrogen atmosphere and cooled to -78°C . A 1.6 M solution of *n*-butyllithium in hexanes (1.27 mL, 2.04 mmol) was added, followed after 4 minutes by DMF (157 μL , 2.04 mmol). After 15 minutes, methanol (1.85 mL) and acetic acid (124 μL) were added and the mixture was allowed to return to room temperature. Water and ethyl acetate were added. The organic layer was dried over sodium sulfate, concentrated *in vacuo* and purified by flash chromatography on silica (FlashPack, eluent: DCM –*n*-heptane (1 : 1) \rightarrow DCM) to give 384 mg (75%) of 4-((tert-butyldimethylsilyloxy)methyl)picolinaldehyde as a colourless liquid. ^1H NMR (CDCl_3): 10.10 (s, 1H), 8.74 (d, $J = 4.9$, 1H), 7.90 (s, 1H), 7.53 (m, 1H), 4.82 (s, 2H), 0.96 (s, 9H), 0.13 (s, 6H); ^{13}C NMR (CDCl_3): 193.4, 152.7, 152.3, 150.1, 124.8, 118.6, 63.3, 25.8, 18.3, -5.4 ; HR-ESI-MS: calculated for $[\text{C}_{13}\text{H}_{21}\text{NO}_2\text{Si} + \text{H}]^+$ 252.1420, found 252.1408.

(E)-(2-(2-((4-((tert-Butyldimethylsilyloxy)methyl)pyridin-2-yl)-methylene)-1-methylhydrazinyl)pyridin-4-yl)methanol 4-Me. 8-Me (238 mg, 1.55 mmol) was placed in a flask under a nitrogen atmosphere. A solution of **9** (389 mg, 1.55 mmol) in CHCl_3 (40 mL) was added and the mixture was stirred at room temperature for 24 hours. The reaction mixture was then concentrated *in vacuo* and purified by flash chromatography on silica (eluent: $\text{DCM} \rightarrow 5\%$ MeOH) to give 489 mg (82%) of a light reddish solid. ^1H NMR (CDCl_3): 8.39 (d, $J = 4.9$, 1H), 8.11 (d, $J = 5.4$, 1H), 7.84 (s, 1H), 7.62 (s, 2H), 7.10 (d, $J = 5.4$, 1H), 6.82 (d, $J = 5.4$, 1H), 4.71 (s, 2H), 4.67 (s, 2H), 4.54 (br. s, 1H), 3.55 (s, 3H), 0.93 (s, 9H), 0.09 (s, 6H); ^{13}C NMR (CDCl_3): 157.4, 154.8, 152.1, 151.2, 148.6, 146.9, 134.2, 119.5, 116.0, 114.1, 107.1, 63.6, 63.5, 29.7, 25.8, 18.3, -5.4 ; HR-ESI-MS: calculated for $[\text{C}_{20}\text{H}_{30}\text{N}_4\text{O}_2\text{Si} + \text{H}]^+$ 387.2211, found 387.2164; elemental analysis: calculated for $[\text{C}_{20}\text{H}_{30}\text{N}_4\text{O}_2\text{Si}]$ C 62.14, H 7.82, N 14.49, found C 61.64, H 7.94, N 14.85.

(E)-(2-(2-((4-((tert-Butyldimethylsilyloxy)methyl)pyridin-2-yl)-methylene)hydrazinyl)pyridin-4-yl)methanol 4-H. 8-H (624 mg, 4.48 mmol) was placed in a flask under a nitrogen atmosphere. A solution of **9** (1.13 g, 4.48 mmol) in CHCl_3 (120 mL) was added and the mixture was stirred at room temperature for

24 hours. The reaction mixture was then concentrated *in vacuo* and purified by recrystallization in diethyl ether. 1.28 g (77%) of a white-off solid were collected. ^1H NMR (CD_3OD): 8.42 (d, $J = 5.2$, 1H), 8.10 (s, 1H), 8.05 (d, $J = 5.2$, 1H), 8.00 (s, 1H), 7.36 (s, 1H), 7.30 (d, $J = 5.2$, 1H), 6.87 (d, $J = 5.6$, 1H), 4.86 (s, 2H), 4.64 (s, 2H), 1.01 (s, 9H, CH_3), 0.18 (s, 6H, SiCH_3); ^{13}C NMR (CD_3OD): 158.2, 155.8, 155.2, 153.8, 149.6, 148.4, 139.7, 121.6, 117.9, 114.9, 106.0, 64.6, 64.0, 26.5, 19.6, -5.2 ; ESI-MS: calculated for $[\text{C}_{19}\text{H}_{28}\text{N}_4\text{O}_2\text{Si} + \text{H}]^+$ 373.2060, found 373.3378.

(E)-(2-((2-(4-(Hydroxymethyl)pyridin-2-yl)-2-methylhydrazono)-methyl)pyridin-4-yl)methanol 5-Me. 4-Me (155 mg, 0.40 mmol) was dissolved in THF (20 mL) under a nitrogen atmosphere in an ice bath. Tetrabutylammonium fluoride (1M in THF, 0.44 mL, 0.44 mmol) was then added. After 4 hours, EtOAc and H_2O were added. The aqueous layer was extracted twice with EtOAc. The organic layers were combined, dried over sodium sulfate and concentrated *in vacuo*. DCM was added to the residue. The mixture was sonicated and filtered to give 88 mg (81%) of a beige solid. ^1H NMR (CDCl_3 – CD_3OD (1 : 1)): 8.42 (d, $J = 4.9$, 1H), 8.12 (d, $J = 5.4$, 1H), 8.04 (s, 1H), 7.78 (s, 1H), 7.71 (s, 1H), 7.24 (d, $J = 4.4$, 1H), 6.85 (d, $J = 5.4$, 1H), 4.71 (s, 2H), 4.66 (s, 2H), 3.65 (s, 3H); ^{13}C NMR (CDCl_3 – CD_3OD (1 : 1)): 158.4, 155.6, 153.5, 152.9, 149.0, 147.3, 134.1, 121.1, 117.7, 115.1, 108.2, 63.7, 63.2, 30.4; HR-ESI-MS: calculated for $[\text{C}_{14}\text{H}_{16}\text{N}_4\text{O}_2 + \text{H}]^+$ 273.1346, found 273.1361.

(E)-(2-((2-(4-(Hydroxymethyl)pyridin-2-yl)hydrazono)methyl)-pyridin-4-yl)methanol 5-H. 4-H (500 mg, 1.34 mmol) was dissolved in THF (65 mL) under a nitrogen atmosphere and cooled to 0°C using an ice bath. Tetrabutylammonium fluoride (1M in THF, 1.47 mL, 1.47 mmol) was then added. After 4 hours, EtOAc and H_2O were added. The aqueous layer was extracted twice with EtOAc. The organic layers were combined, dried over sodium sulfate and concentrated *in vacuo*. Recrystallization from a CHCl_3 – Et_2O mixture gave 340 mg (quantitative) of a beige solid. ^1H NMR (CDCl_3 – CD_3OD (1 : 1)): 8.40 (d, $J = 5.2$, 1H), 8.02 (m, 2H), 7.56 (br, 1H), 7.35 (s, 1H), 7.27 (d, $J = 5.2$, 1H), 6.81 (d, $J = 5.6$, 1H), 4.70 (s, 2H), 4.64 (s, 2H); ^{13}C NMR (CDCl_3 – CD_3OD (1 : 1)): 157.2, 154.8, 154.3, 152.9, 149.0, 147.7, 139.1, 121.4, 118.1, 114.5, 105.6, 63.5, 63.2.

(E)-(2-((2-(4-Formylpyridin-2-yl)-2-methylhydrazono)methyl)-isonicotinaldehyde 2. 5-Me (84 mg, 0.31 mmol) and Dess–Martin periodinane (313 mg, 0.74 mmol) were placed in a flask under a nitrogen atmosphere. DCM (16 mL) was added and the mixture was stirred at room temperature for 8 hours. A saturated solution of NaHCO_3 and $\text{Na}_2\text{S}_2\text{O}_3$ (1.3 g) was then added and the heterogeneous solution was stirred vigorously overnight. The organic layer was washed twice with a saturated solution of NaHCO_3 . The organic layer was dried over sodium sulfate and concentrated *in vacuo* to give a quantitative light yellow solid. ^1H NMR (CDCl_3): 10.18 (s, 1H), 10.12 (s, 1H), 8.80 (d, $J = 4.9$, 1H), 8.44 (d, $J = 4.9$, 1H), 8.39 (s, 1H), 8.12 (s, 1H), 7.89 (s, 1H), 7.62 (d, $J = 4.9$, 1H), 7.25 (d, $J = 4.9$, 1H), 3.76 (s, 3H); ^1H NMR (500 MHz, CDCl_3 – CD_3CN (6 : 4)): 10.16 (s, 1H, H_5), 10.11

(s, 1H, H₈), 8.78 (dd, $J = 4.0$, $J = 0.4$, 1H, H₃), 8.42 (m, 2H, H₆ + H₁₀), 8.17 (dd, $J = 1.2$, $J = 0.8$, 1H, H₇), 7.90 (d, $J = 0.4$, 1H, H₂), 7.62 (dd, $J = 4.0$, $J = 1.2$, 1H, H₄), 7.23 (dd, $J = 4.0$, $J = 0.8$, 1H, H₉), 3.74 (d, $J = 0.8$, 3H, H₁); ¹³C NMR (CDCl₃): 191.9, 191.5, 158.4, 156.7, 150.6, 148.5, 143.7, 142.1, 135.3 (CH₂), 120.1, 119.0 (CH₆), 113.7, 110.9, 30.2; HR-ESI-MS: calculated for [C₁₄H₁₂N₄O₂ + Li]⁺ 275.1115, found 275.1083.

2-Bromo-4-((*tert*-butyldimethylsilyloxy)methyl)pyridine 10.

To a solution of (2-bromopyridin-4-yl)methanol (500 mg, 2.66 mmol) in DCM (23 mL), cooled to 0 °C using an ice bath and placed under a nitrogen atmosphere, was added DMAP (357 mg, 2.93 mmol). After 5 minutes, *tert*-butyldimethylsilyl chloride (441 mg, 2.93 mmol) was added, the mixture was allowed to return to room temperature, with stirring, overnight. The reaction mixture was washed twice with water. The organic layer was dried over sodium sulfate, concentrated *in vacuo*, and purified by flash chromatography on silica (eluent: DCM) to give 742 mg (93%) of 2-bromo-4-((*tert*-butyldimethylsilyloxy)methyl)pyridine as a colourless liquid. ¹H NMR (CDCl₃): 8.30 (d, $J = 5.4$, 1H), 7.46 (s, 1H), 7.19 (m, 1H), 4.71 (s, 2H), 0.95 (s, 9H), 0.12 (s, 6H); ¹³C NMR (CDCl₃): 153.8, 149.8, 142.4, 124.9, 119.8, 62.9, 25.8, 18.3, -5.4; HR-ESI-MS: calculated for [C₁₂H₂₀BrNOSi + H]⁺ 302.0570, found 302.0541; elemental analysis: calculated for [C₁₂H₂₀BrNOSi] C 47.68, H 6.67, N 4.63, found C 47.46, H 6.23, N 4.37.

(6-Bromopyridin-2-yl)methanol 11. The product was prepared using a modified literature procedure.⁷¹ To a solution of *n*-butyllithium (1.6 M in hexanes, 8.05 mL, 12.89 mmol) in anhydrous THF (7.7 mL) at -78 °C was slowly added a solution of 2,6-dibromopyridine (3.05 g, 12.89 mmol) in anhydrous THF (18 mL) while keeping the internal temperature below -70 °C. The addition required 3 hours. The green solution was then stirred for an additional 10 minutes and anhydrous DMF (1.54 mL, 19.97 mmol) was slowly added. The reaction mixture was stirred for 15 minutes. Methanol (12.9 mL) and acetic acid (0.82 mL), followed by sodium borohydride (488 mg, 12.89 mmol), were added and the reaction mixture was allowed to return to room temperature overnight. 40 mL of a saturated solution of NH₄Cl were added to the yellow solution. The aqueous layer was extracted twice with EtOAc. The organic layer was then washed with brine, dried over sodium sulfate and concentrated under vacuum. Purification by flash chromatography on silica (eluent: DCM → 20% EtOAc) yielded 1.99 g (82%) of a light-yellow liquid. ¹H NMR (CDCl₃): 7.55 (t, $J = 7.6$, 1H), 7.39 (d, $J = 7.6$, 1H), 7.28 (dd, $J = 7.6$, $J = 0.8$, 1H), 4.75 (d, $J = 5.6$, 2H, CH₂), 3.10–3.20 (br, 1H, OH); ¹³C NMR (CDCl₃): 161.1, 141.4, 139.0, 126.7, 119.2, 64.2; HR-ESI-MS: calculated for [C₆H₆BrNO + H]⁺ 187.9711, found 187.9699, [C₆H₆BrNO + Li]⁺ 193.9793, found 193.9782, [C₆H₆BrNO + Na]⁺ 209.9530, found 209.9516.

Zn-1-Me. Anhydrous Zn(OTf)₂ (50 µL of a 60 mM solution in CDCl₃*-CD₃CN (6 : 4), 3 µmol) was added to a 5 mM solution of the **1-Me** (0.805 mg, 3 µmol) in CDCl₃*-CD₃CN

(6 : 4) (0.6 mL). ¹H NMR (CDCl₃*-CD₃CN (6 : 4)): 10.17 (s, 1H, H₃), 10.06 (s, 1H, H₁₀), 8.47 (t, $J = 7.8$, 1H, H₅), 8.32 (t, $J = 7.8$, 2H, H₄ and H₈), 8.21 (s, 1H, H₂), 8.14 (d, $J = 7.6$, 1H, H₆), 7.93 (d, $J = 7.2$, 1H, H₉), 7.72 (d, $J = 8.8$, 1H, H₇), 3.75 (s, 3H, H₁); MALDI-TOF (dithranol): calculated for [C₁₅H₁₂F₃N₄O₅SZn]⁺ 480.9772, found 480.9427.

Pb-1-Me. Anhydrous Pb(OTf)₂ (50 µL of a 60 mM solution in CD₃CN, 3 µmol) was added to a 5 mM solution of the **1-Me** (0.805 mg, 3 µmol) in CDCl₃*-CD₃CN (6 : 4) (0.6 mL). ¹H NMR (CDCl₃*-CD₃CN (55 : 45)): 10.50 (s, 1H), 10.46 (s, 1H), 8.63 (s, 1H), 8.49 (t, $J = 7.8$, 1H), 8.34–8.27 (m, 2H), 8.18 (dd, $J = 8.0$, $J = 0.8$, 1H), 7.94 (d, $J = 7.2$, 1H), 7.73 (d, $J = 8.8$, 1H), 3.77 (s, 3H); MALDI-TOF (dithranol): calculated for [C₁₅H₁₂F₃N₄O₅PbS]⁺ 625.0247, found 624.8891.

Zn-2. Anhydrous Zn(OTf)₂ (50 µL of a 60 mM solution in CDCl₃*-CD₃CN (6 : 4), 3 µmol) was added to a 5 mM solution of the **2** (0.805 mg, 3 µmol) in CDCl₃*-CD₃CN (6 : 4) (0.6 mL). ¹H NMR (CDCl₃*-CD₃CN (6 : 4)): 10.08 (s, 1H, H₅), 10.04 (s, 1H, H₈), 8.63 (s, 1H, H₂), 8.34 (d, $J = 5.2$, 1H, H₃), 8.28 (s, 1H, H₆), 7.96 (d, $J = 5.2$, 1H, H₁₀), 7.84 (s, 1H, H₇), 7.80 (dd, $J = 5.2$, $J = 1.2$, 1H, H₄), 7.35 (d, $J = 5.6$, 1H, H₉), 4.01 (s, 3H, H₁).

Zn-2. Anhydrous Zn(OTf)₂ (50 µL of a 60 mM solution in CDCl₃*-CD₃CN (6 : 4), 3 µmol) was added to a 5 mM solution of the **2** (0.805 mg, 3 µmol) in CDCl₃*-CD₃CN (6 : 4) (0.6 mL). ¹H NMR (CDCl₃*-CD₃CN (6 : 4)): 10.19 (s, 1H, H₅), 10.14 (s, 1H, H₈), 8.95 (d, $J = 5.2$, 1H, H₃), 8.60 (d, $J = 5.2$, 1H, H₁₀), 8.19 (s, 1H, H₆), 8.15 (s, 1H, H₂), 8.09 (dd, $J = 5.2$, $J = 1.2$, 1H, H₄), 7.78 (s, 1H, H₇), 7.65 (d, $J = 5.6$, 1H, H₉), 3.77 (s, 3H, H₁); MALDI-TOF (dithranol): calculated for [C₁₅H₁₂F₃N₄O₅SZn]⁺ 480.9772, found 480.9705.

Pb-2. Anhydrous Pb(OTf)₂ (50 µL of a 60 mM solution in CD₃CN (6 : 4), 3 µmol) was added to a 5 mM solution of the **2** (0.805 mg, 3 µmol) in CDCl₃*-CD₃CN (6 : 4) (0.6 mL). ¹H NMR (CDCl₃*-CD₃CN (55 : 45)): 10.16 (s, 1H), 10.11 (s, 1H), 9.12 (d, $J = 5.2$, 1H), 8.71 (d, $J = 5.6$, 1H), 8.64 (s, 1H), 8.27 (s, 1H), 8.07 (dd, $J = 5.2$, $J = 1.6$, 1H), 7.79 (s, 1H), 7.61 (dd, $J = 5.2$, $J = 1.2$, 1H), 3.76 (s, 3H, CH₃); MALDI-TOF (dithranol): calculated for [C₁₅H₁₂F₃N₄O₅PbS]⁺ 625.0247, found 624.9398.

9₂-(N₂C₂)₂. 1,2-Diaminoethane (50 µL of a 60 mM solution in CDCl₃*-CD₃CN (6 : 4), 3 µmol) was added to a 5 mM solution of **9** (0.805 mg, 3 µmol) in CDCl₃*-CD₃CN (6 : 4) (0.6 mL). A precipitate formed. ¹H NMR showed no starting material was left in the solution. Direct analysis of the precipitate by MALDI-TOF (THAP): calculated for [C₃₂H₃₂N₁₂ + H]⁺ 585.285, found 585.200.

1-(NC₈)₂. 1-Aminooctane (50 µL of a 120 mM solution in CDCl₃*-CD₃CN (6 : 4), 6 µmol) was added to a 5 mM solution of **1-Me** (0.805 mg, 3 µmol) in CDCl₃*-CD₃CN (6 : 4) (0.6 mL). Thermodynamic equilibrium was reached after 4–6 hours when the sample was left standing without stirring. ¹H NMR (CDCl₃*-CD₃CN (6 : 4)): 8.34 (s, 1H), 8.24

(s, 1H), 8.04 (dd, $J = 7.2$, $J = 2.4$, 1H), 7.81–7.75 (m, 4H), 7.68 (t, $J = 7.8$, 1H), 7.47 (dd, $J = 7.6$, $J = 0.8$, 1H), 3.72 (s, 3H, NCH_3), 3.67–3.60 (m, 4H), 1.68 (m, 4H), 1.34–1.26 (m, 20H), 0.85 (t, $J = 6.8$, 6H); MALDI-TOF (dithranol): calculated for $[\text{C}_{30}\text{H}_{46}\text{N}_6 + \text{H}]^+$ 491.386, found 491.344.

$\text{I}_2(\text{N}_2\text{O})_2$. 1,5-Diamino-3-oxapentane (50 μL of a 60 mM solution in $\text{CDCl}_3^*-\text{CD}_3\text{CN}$ (6 : 4), 3 μmol) was added to a 5 mM solution of **1-Me** (0.805 mg, 3 μmol) in $\text{CDCl}_3^*-\text{CD}_3\text{CN}$ (6 : 4) (0.6 mL). Thermodynamic equilibrium was reached after 3 hours when the sample was left standing without stirring. ^1H NMR ($\text{CDCl}_3^*-\text{CD}_3\text{CN}$ (6 : 4)): 8.07 (s, 1H), 8.05 (s, 1H), 7.96 (s, 1H), 7.94 (s, 1H), 7.76 (m, 2H), 7.47–7.38 (m, 8H), 7.36–7.30 (m, 2H), 7.17 (d, $J = 6.8$, 1H), 7.12 (d, $J = 6.8$, 1H), 3.73 (m, 16H), 3.51 (s, 3H), 3.48 (s, 3H); MALDI-TOF: calculated for $[\text{C}_{36}\text{H}_{40}\text{N}_{12}\text{O}_2 + \text{H}]^+$ 673.348, found 673.378.

$2(\text{NC}_8)_2$. 1-Aminooctane (50 μL of a 120 mM solution in $\text{CDCl}_3^*-\text{CD}_3\text{CN}$ (6 : 4), 6 μmol) was added to a 5 mM solution of **2** (0.805 mg, 3 μmol) in $\text{CDCl}_3^*-\text{CD}_3\text{CN}$ (6 : 4) (0.6 mL). Thermodynamic equilibrium was reached after 6–7 hours when the sample was left standing without stirring. ^1H NMR ($\text{CDCl}_3^*-\text{CD}_3\text{CN}$ (6 : 4)): 8.58 (d, $J = 5.2$, 1H), 8.36 (s, 1H), 8.32 (s, 1H), 8.23 (m, 2H), 7.95 (s, 1H), 7.80 (s, 1H), 7.54 (dd, $J = 5.2$, $J = 1.6$, 1H), 7.20 (dd, $J = 5.2$, $J = 1.2$, 1H), 3.69 (s, 3H), 3.65 (q, $J = 5.5$, 4H, NCH_2), 1.69 (m, 4H), 1.31 (m, 20H), 0.84 (m, 6H).

$2_2(\text{N}_2\text{C}_3)_2$. 1,3-Diaminopropane (50 μL of a 60 mM solution in $\text{CDCl}_3^*-\text{CD}_3\text{CN}$ (6 : 4), 3 μmol) was added to a 5 mM solution of **2** (0.805 mg, 3 μmol) in $\text{CDCl}_3^*-\text{CD}_3\text{CN}$ (6 : 4) (0.6 mL). ^1H NMR ($\text{CDCl}_3^*-\text{CD}_3\text{CN}$ (6 : 4)): 8.53 (dd, $J = 8.4$, $J = 5.2$, 1H), 8.42 (s, 1H), 8.39 (s, 1H), 8.28 (d, $J = 4.4$, 1H), 8.20 (dd, $J = 8.4$, $J = 5.2$, 1H), 7.97 (d, $J = 4.4$, 1H), 7.73 (d, $J = 1.2$, 1H), 7.45 (m, 1H), 7.12 (dd, $J = 5.2$, $J = 1.2$, 1H), 3.85 (m, 4H, NCH_2), 3.66 (s, 3H, NCH_3), 2.16 (m, 2H). Crystals spontaneously formed. Direct analysis of the solid by MALDI-TOF (THAP): calculated for $[\text{C}_{34}\text{H}_{36}\text{N}_{12} + \text{H}]^+$ 613.326, found 613.341.

$2_2(\text{N}_2\text{C}_3')_2$. $\text{N}_2\text{C}_3'$ (50 μL of a 60 mM solution in $\text{CDCl}_3^*-\text{CD}_3\text{CN}$ (6 : 4), 3 μmol) was added to a 5 mM solution of **2** (0.805 mg, 3 μmol) in $\text{CDCl}_3^*-\text{CD}_3\text{CN}$ (6 : 4) (0.6 mL). Thermodynamic equilibrium was reached after 2 days at room temperature. ^1H NMR ($\text{CDCl}_3^*-\text{CD}_3\text{CN}$ (6 : 4)): 8.55 (d, $J = 4.8$, 1H), 8.45 (br, 1H), 8.39 (br, 2H), 8.22 (d, $J = 5.2$, 1H), 8.09 (d, $J = 10.0$, 1H), 7.74 (s, 1H), 7.49 (m, 1H), 7.16 (m, 1H), 3.92 (br, 4H, NCH_2), 3.66 (s, 3H, NCH_3), 1.29–0.81 (m, 18H); MALDI-TOF (dithranol): calculated for $[\text{C}_{50}\text{H}_{68}\text{N}_{12} + \text{H}]^+$ 837.5768, found 837.5252.

$2_2(\text{N}_2\text{C}_4)_2$. *Preparation in $\text{CDCl}_3-\text{CD}_3\text{CN}$ mixture:* 1,4-diaminobutane (50 μL of a 60 mM solution in $\text{CDCl}_3^*-\text{CD}_3\text{CN}$ (6 : 4), 3 μmol) was added to a 5 mM solution of **2** (0.805 mg, 3 μmol) in $\text{CDCl}_3^*-\text{CD}_3\text{CN}$ (6 : 4) (0.6 mL). A precipitate formed. Direct analysis of the precipitate by MALDI-TOF (THAP): calculated for $[\text{C}_{36}\text{H}_{40}\text{N}_{12} + \text{H}]^+$ 641.357, found 641.346. *Preparation in CDCl_3 :* 1,4-diaminobutane (50 μL of a 60 mM solution in CDCl_3^* , 3 μmol) was

added to a 5 mM solution of **2** (0.805 mg, 3 μmol) in CDCl_3^* (0.6 mL). Thermodynamic equilibrium was reached after 12–24 hours. ^1H NMR (CDCl_3^*): 8.63 (d, $J = 5.2$, 1H), 8.43 (d, $J = 4.4$, 1H), 8.39 (d, $J = 1.2$, 1H), 8.36 (d, $J = 1.6$, 1H), 8.30 (d, $J = 5.2$, 1H), 8.11 (d, $J = 5.2$, 1H), 7.82 (s, 1H), 7.49 (ddd, $J = 10.0$, $J = 5.2$, $J = 1.6$, 1H), 7.18 (ddd, $J = 10.0$, $J = 5.2$, $J = 1.6$, 1H), 3.78 (m, 4H), 3.73 (s, 3H, CH_3), 1.91 (m, 4H); MALDI-TOF: calculated for $[\text{C}_{36}\text{H}_{40}\text{N}_{12} + \text{H}]^+$ 641.3577, found 641.2272.

$2\text{-N}_2\text{C}_5$. 1,5-Diaminopentane (50 μL of a 60 mM solution in $\text{CDCl}_3^*-\text{CD}_3\text{CN}$ (6 : 4), 3 μmol) was added to a 5 mM solution of **2** (0.805 mg, 3 μmol) in $\text{CDCl}_3^*-\text{CD}_3\text{CN}$ (6 : 4) (0.6 mL). Thermodynamic equilibrium was reached after 3–4 hours when the sample was left standing without stirring. ^1H NMR ($\text{CDCl}_3^*-\text{CD}_3\text{CN}$ (6 : 4)): 8.72 (s, 1H), 8.57 (d, $J = 5.2$, 1H), 8.40 (s, 1H, H_8 or H_5), 8.39 (s, 1H, H_5 or H_8), 8.35 (s, 1H), 8.26 (d, $J = 5.2$, 1H), 7.71 (s, 1H, H_2), 7.23 (dd, $J = 4.8$, $J = 1.6$, 1H), 6.89 (dd, $J = 5.2$, $J = 1.6$, 1H), 3.69 (m, 4H, NCH_2), 3.65 (s, 3H, H_1), 2.09 (m, 2H), 1.72 (m, 4H); MALDI-TOF (dithranol): calculated for $[\text{C}_{19}\text{H}_{22}\text{N}_6 + \text{H}]^+$ 335.1984, found 335.2013.

$2_2(\text{N}_2\text{O})_2$. 1,5-Diamino-3-oxapentane (50 μL of a 60 mM solution in $\text{CDCl}_3^*-\text{CD}_3\text{CN}$ (6 : 4), 3 μmol) was added to a 5 mM solution of **2** (0.805 mg, 3 μmol) in $\text{CDCl}_3^*-\text{CD}_3\text{CN}$ (6 : 4) (0.6 mL). Thermodynamic equilibrium was reached after 3–4 hours when the sample was left standing without stirring. ^1H NMR ($\text{CDCl}_3^*-\text{CD}_3\text{CN}$ (6 : 4)): 8.84 (s, 1H), 8.57 (d, $J = 4.8$, 1H), 8.52 (s, 1H), 8.39 (s, 1H), 8.35 (s, 1H), 8.27 (d, $J = 4.8$, 1H), 7.69 (s, 1H), 7.24 (dd, $J = 4.8$, $J = 1.2$, 1H), 6.91 (dd, $J = 4.8$, $J = 1.2$, 1H), 3.88 (m, 4H), 3.75 (m, 4H), 3.64 (s, 3H); MALDI-TOF (dithranol): calculated for $[\text{C}_{36}\text{H}_{40}\text{N}_{12}\text{O}_2 + \text{H}]^+$ 673.347, found 673.303.

$\text{Zn-1-Me-N}_2\text{C}_4$. Anhydrous $\text{Zn}(\text{OTf})_2$ (50 μL of a 60 mM solution in $\text{CDCl}_3^*-\text{CD}_3\text{CN}$ (6 : 4), 3 μmol) was added to a 5 mM solution of **1-Me** (0.805 mg, 3 μmol) in $\text{CDCl}_3^*-\text{CD}_3\text{CN}$ (6 : 4) (0.6 mL). 1,4-Diaminobutane (50 μL of a 60 mM solution in $\text{CDCl}_3^*-\text{CD}_3\text{CN}$ (6 : 4), 3 μmol) was then added. Thermodynamic equilibrium was reached after 2–3 hours when the sample was left standing without stirring. ^1H NMR ($\text{CDCl}_3^*-\text{CD}_3\text{CN}$ (6 : 4)): 8.58 (s, 1H), 8.50 (s, 1H), 8.21 (t, $J = 7.6$, 1H), 8.08 (dd, $J = 8.4$, $J = 7.2$, 1H), 7.99 (s, 1H), 7.83 (dd, $J = 7.6$, $J = 0.8$, 1H), 7.76 (dd, $J = 7.6$, $J = 1.2$, 1H), 7.44 (d, $J = 8.4$, 1H), 7.38 (d, $J = 6.8$, 1H), 3.97–3.93 (m, 4H), 3.66 (s, 3H), 1.99 (m, 4H); MALDI-TOF (dithranol): calculated for $[\text{C}_{19}\text{H}_{20}\text{F}_3\text{N}_6\text{O}_3\text{SZn}]^+$ 533.0561, found 533.0075.

$\text{Zn-1-Oct-N}_2\text{C}_4$. Anhydrous $\text{Zn}(\text{OTf})_2$ (50 μL of a 500 mM solution in CD_3CN , 25 μmol) was added to a 50 mM solution of **1-Oct** (9.162 mg, 25 μmol) and 1,4-diaminobutane (2.204 mg, 25 μmol) in $\text{CDCl}_3^*-\text{CD}_3\text{CN}$ (8 : 2) (0.5 mL). Thermodynamic equilibrium was reached after a few hours when the sample was left standing without stirring. ^1H NMR ($\text{CDCl}_3^*-\text{CD}_3\text{CN}$ (73 : 27)): 8.53 (s, 1H), 8.46 (s, 1H), 8.15 (t, $J = 7.8$, 1H), 8.02 (t, $J = 7.8$, 1H), 7.94 (s, 1H), 7.79 (d, $J = 7.6$, 1H), 7.69 (d, $J = 7.6$, 1H), 7.32 (t, $J = 8.0$, 2H), 4.08 (t, $J = 7.8$, 2H), 3.94 (m, 4H), 1.98 (m, 4H), 1.76–1.17

(m, 12H), 0.85 (m, 3H); MALDI-TOF (dithranol): calculated for $[\text{C}_{26}\text{H}_{34}\text{F}_3\text{N}_6\text{O}_3\text{SZn}]^+$ 631.1657, found 631.0243.

Zn-1-Me-N₂C₅. Anhydrous $\text{Zn}(\text{OTf})_2$ (50 μL of a 60 mM solution in $\text{CDCl}_3^*-\text{CD}_3\text{CN}$ (6 : 4), 3 μmol) was added to a 5 mM solution of **1-Me** (0.805 mg, 3 μmol) in $\text{CDCl}_3^*-\text{CD}_3\text{CN}$ (6 : 4) (0.6 mL). 1,5-Diaminopentane (50 μL of a 60 mM solution in $\text{CDCl}_3^*-\text{CD}_3\text{CN}$ (6 : 4), 3 μmol) was then added. Thermodynamic equilibrium was reached after a few hours when the sample was left standing without stirring. ^1H NMR ($\text{CDCl}_3^*-\text{CD}_3\text{CN}$ (6 : 4)): 8.56 (s, 1H), 8.48 (s, 1H), 8.22 (t, $J = 7.6$, 1H), 8.09 (m, 2H), 7.86 (dd, $J = 7.6$, $J = 1.2$, 1H), 7.76 (dd, $J = 7.6$, $J = 0.8$, 1H), 7.45 (d, overlapped with solvent peak, 1H), 7.39 (d, $J = 7.2$, 1H), 4.15–4.08 (m, 4H), 3.67 (s, 3H), 2.30–1.70 (m, 6H); HR-ESI-MS: calculated for $[\text{C}_{20}\text{H}_{22}\text{F}_3\text{N}_6\text{O}_3\text{SZn}]^+$ 547.071, found 547.039.

Zn-1-Oct-N₂C₅. Anhydrous $\text{Zn}(\text{OTf})_2$ (50 μL of a 500 mM solution in CD_3CN , 25 μmol) was added to a 50 mM solution of **1-Oct** (9.162 mg, 25 μmol) and 1,5-diaminopentane (2.555 mg, 25 μmol) in $\text{CDCl}_3^*-\text{CD}_3\text{CN}$ (8 : 2) (0.5 mL). Thermodynamic equilibrium was reached after 8 hours when the sample was left standing without stirring. ^1H NMR ($\text{CDCl}_3^*-\text{CD}_3\text{CN}$ (73 : 27)): 8.53 (s, 1H), 8.45 (s, 1H), 8.17 (t, $J = 7.6$, 1H), 8.03 (m, 2H), 7.83 (d, $J = 7.6$, 1H), 7.71 (d, $J = 7.6$, 1H), 7.34 (m, 2H), 4.11 (br, 6H), 3.03 (br, 4H), 1.99–0.85 (m, 17H); MALDI-TOF (dithranol): calculated for $[\text{C}_{27}\text{H}_{36}\text{F}_3\text{N}_6\text{O}_3\text{SZn}]^+$ 645.1813, found 645.0073.

Zn-1-Me-N₂O. Anhydrous $\text{Zn}(\text{OTf})_2$ (50 μL of a 60 mM solution in $\text{CDCl}_3^*-\text{CD}_3\text{CN}$ (6 : 4), 3 μmol) was added to a 5 mM solution of **1-Me** (0.805 mg, 3 μmol) in $\text{CDCl}_3^*-\text{CD}_3\text{CN}$ (6 : 4) (0.6 mL). 1,5-Diamino-3-oxapentane (50 μL of a 60 mM solution in $\text{CDCl}_3^*-\text{CD}_3\text{CN}$ (6 : 4), 3 μmol) was then added. Thermodynamic equilibrium was reached after a few hours when the sample was stirred. ^1H NMR ($\text{CDCl}_3^*-\text{CD}_3\text{CN}$ (6 : 4)): 8.59 (s, 1H), 8.50 (s, 1H), 8.23 (t, $J = 7.8$, 1H), 8.12–8.08 (m, 2H), 7.86 (d, $J = 8.0$, 1H), 7.80 (d, $J = 6.8$, 1H), 7.46 (d, $J = 8.8$, 1H), 7.42 (d, $J = 7.2$, 1H), 4.26–4.21 (m, 4H), 4.05 (t, $J = 5.4$, 2H), 3.96 (t, $J = 5.4$, 2H), 3.69 (s, 3H); MALDI-TOF (dithranol): calculated for $[\text{C}_{19}\text{H}_{20}\text{F}_3\text{N}_6\text{O}_4\text{SZn}]^+$ 549.0510, found 548.9275.

Pb-1-Me-N₂O₂. Anhydrous $\text{Pb}(\text{OTf})_2$ (50 μL of a 60 mM solution in CD_3CN , 3 μmol) was added to a 5 mM solution of **1-Me** (0.805 mg, 3 μmol) in $\text{CDCl}_3^*-\text{CD}_3\text{CN}$ (6 : 4) (0.6 mL). 1,2-Bis(2-aminoethoxy)ethane (50 μL of a 60 mM solution in $\text{CDCl}_3^*-\text{CD}_3\text{CN}$ (6 : 4), 3 μmol) was then added. Thermodynamic equilibrium was reached after 12–24 hours when the sample was left standing without stirring. ^1H NMR ($\text{CDCl}_3^*-\text{CD}_3\text{CN}$ (56 : 44)): 9.01 (s, 1H), 8.97 (s, 1H), 8.33 (s, 1H), 8.20 (t, $J = 7.6$, 1H), 8.05 (t, $J = 8.0$, 1H), 7.86 (d, $J = 8.0$, 1H), 7.80 (d, $J = 7.6$, 1H), 7.43–7.40 (m, 2H), 4.12 (m, 4H), 3.96–3.91 (m, 4H), 3.69 (br, 7H); MALDI-TOF (dithranol): calculated for $[\text{C}_{21}\text{H}_{24}\text{F}_3\text{N}_6\text{O}_5\text{PbS}]^+$ 737.1247, found 737.0421.

Pb-1-Me-N₂O₃. Anhydrous $\text{Pb}(\text{OTf})_2$ (50 μL of a 60 mM solution in CD_3CN , 3 μmol) was added to a 5 mM solution of **1-Me** (0.805 mg, 3 μmol) in $\text{CDCl}_3^*-\text{CD}_3\text{CN}$ (6 : 4) (0.6 mL). 4,7,10-Trioxa-1,13-tridecanediamine (50 μL of a 60 mM

solution in $\text{CDCl}_3^*-\text{CD}_3\text{CN}$ (6 : 4), 3 μmol) was then added. Thermodynamic equilibrium was reached after 12–24 hours when the sample was left standing without stirring. ^1H NMR ($\text{CDCl}_3^*-\text{CD}_3\text{CN}$ (56 : 44)): 9.03 (s, 2H), 8.40 (s, 1H), 8.25 (t, $J = 7.8$, 1H), 8.09 (t, $J = 8.0$, 1H), 7.92 (d, $J = 7.2$, 1H), 7.84 (d, $J = 7.6$, 1H), 7.46–7.44 (m, 2H), 4.10 (m, 4H), 3.71 (m, 8H), 3.59 (br, 7H), 2.05 (m, 4H). MALDI-TOF (dithranol): calculated for $[\text{C}_{25}\text{H}_{32}\text{F}_3\text{N}_6\text{O}_6\text{PbS}]^+$ 809.1822, found 808.9672.

Pb-1-Oct-N₂O₃. Anhydrous $\text{Pb}(\text{OTf})_2$ (50 μL of a 500 mM solution in CD_3CN , 25 μmol) was added to a 50 mM solution of **1-Oct** (9.162 mg, 25 μmol) and 4,7,10-trioxa-1,13-tridecanediamine (5.508 mg, 25 μmol) in $\text{CDCl}_3^*-\text{CD}_3\text{CN}$ (6 : 4) (0.5 mL). Thermodynamic equilibrium was reached after 12 hours when the sample was left standing without stirring. ^1H NMR ($\text{CDCl}_3^*-\text{CD}_3\text{CN}$ (55 : 45)): 9.04 (s, 2H), 8.39 (s, 1H), 8.27 (t, $J = 7.6$, 1H), 8.09 (t, $J = 8.0$, 1H), 7.96 (d, $J = 7.6$, 1H), 7.86 (d, $J = 7.6$, 1H), 7.46 (d, $J = 7.6$, 1H), 7.40 (d, $J = 8.8$, 1H), 4.16–0.86 (m, 37H); MALDI-TOF (dithranol): calculated for $[\text{C}_{32}\text{H}_{46}\text{F}_3\text{N}_6\text{O}_6\text{PbS}]^+$ 907.291, found 907.174.

Acknowledgements

We thank Dr S. Jean Candau for discussions concerning the characterization of the polymers, Dr L. Allouche for DOSY NMR measurements, Dr A. Madalan for X-ray crystallographic analyses, Dr M. Elhabiri and Prof. A.-M. Albrecht-Gary for helpful discussions concerning the kinetic analyses, A. Mème and Dr E. Leize-Wagner for solid state MALDI-TOF analyses, Dr J. Dintinger and Prof. T. Ebbesen for scanning electron microscopy determination. Mitsui Chemicals (Dr T. Ono and S. Fujii) is acknowledged for DSC and TGA measurements and the BASF ISIS-group for DSC measurement. SU thanks the French Ministère de la Recherche for a pre-doctoral fellowship.

References

- 1 J.-M. Lehn, *Chem. Soc. Rev.*, 2007, **36**, 151–160.
- 2 S. J. Rowan, S. J. Cantrill, G. R. L. Cousins, J. K. M. Sanders and J. F. Stoddart, *Angew. Chem., Int. Ed.*, 2002, **41**, 898–952.
- 3 J.-M. Lehn, *Supramolecular Chemistry*, Wiley-VCH, Weinheim, 1995.
- 4 J.-M. Lehn, *Proc. Natl. Acad. Sci. U. S. A.*, 2002, **99**, 4763–4768; J.-M. Lehn, *Science*, 2002, **295**, 2400–2403; G. M. Whitesides and B. Grzybowski, *Science*, 2002, **295**, 2418–2421.
- 5 J.-M. Lehn, *Prog. Polym. Sci.*, 2005, **30**, 814–831.
- 6 P. T. Corbett, J. Leclaire, L. Vial, K. R. West, J. L. Wietor, J. K. M. Sanders and S. Otto, *Chem. Rev.*, 2006, **106**, 3652–3711; G. R. L. Cousins, S. A. Poulsen and J. K. M. Sanders, *Curr. Opin. Chem. Biol.*, 2000, **4**, 270–279; J.-M. Lehn, *Chem.-Eur. J.*, 1999, **5**, 2455–2463; A. Ganesan, *Angew. Chem., Int. Ed.*, 1998, **37**, 2828–2831.
- 7 L. Vial, R. F. Ludlow, J. Leclaire, R. Perez-Fernandez and S. Otto, *J. Am. Chem. Soc.*, 2006, **128**, 10253–10257; O. Ramstrom and J.-M. Lehn, *Nat. Rev. Drug Discovery*, 2002, **1**, 26–36; T. Bunyapaiboonsri, O. Ramstrom, S. Lohmann, J.-M. Lehn, L. Peng and M. Goeldner, *ChemBioChem*, 2001, **2**, 438–444; O. Ramstrom and J.-M. Lehn, *ChemBioChem*, 2000, **1**, 41–48; I. Huc and J.-M. Lehn, *Proc. Natl. Acad. Sci. U. S. A.*, 1997, **94**, 2106–2110.
- 8 G. Gasparini, L. J. Prins and P. Scrimin, *Angew. Chem., Int. Ed.*, 2008, **47**, 2475–2479; L. Vial, J. K. M. Sanders and S. Otto, *New J. Chem.*, 2005, **29**, 1001–1003; B. Brisig, J. K. M. Sanders and S. Otto, *Angew. Chem., Int. Ed.*, 2003, **42**, 1270–1273; C. L. Hill and X. Zhang, *Nature*, 1995, **373**, 324–326.

- 9 T. Ono, S. Fujii, T. Nobori and J.-M. Lehn, *Chem. Commun.*, 2007, 46–48.
- 10 T. Ono, S. Fujii, T. Nobori and J.-M. Lehn, *Chem. Commun.*, 2007, 4360–4362.
- 11 J. Heo, Y. M. Jeon and C. A. Mirkin, *J. Am. Chem. Soc.*, 2007, **129**, 7712–7713; J. Ramirez, A. M. Stadler, N. Kyritsakas and J.-M. Lehn, *Chem. Commun.*, 2007, 237–239; M. Schweiger, S. R. Seidel, A. M. Arif and P. J. Stang, *Inorg. Chem.*, 2002, **41**, 2556–2559; P. N. W. Baxter, J.-M. Lehn, G. Baum and D. Fenske, *Chem.–Eur. J.*, 2000, **6**, 4510–4517; M. Fujita, *Acc. Chem. Res.*, 1999, **32**, 53–61.
- 12 K. Oh, K. S. Jeong and J. S. Moore, *Nature*, 2001, **414**, 889–893.
- 13 P. N. W. Baxter, R. G. Khoury, J.-M. Lehn, G. Baum and D. Fenske, *Chem.–Eur. J.*, 2000, **6**, 4140–4148.
- 14 T. Kraus, M. Budesinsky, J. C. Cvacka and J. P. Sauvage, *Angew. Chem., Int. Ed.*, 2006, **45**, 258–261; T. J. Kidd, D. A. Leigh and A. J. Wilson, *J. Am. Chem. Soc.*, 1999, **121**, 1599–1600.
- 15 N. Sreenivasachary and J.-M. Lehn, *Proc. Natl. Acad. Sci. U. S. A.*, 2005, **102**, 5938–5943.
- 16 M. Angelin, A. Fischer and O. Ramstrom, *J. Org. Chem.*, 2008, **73**, 3593–3595; C. F. Chow, S. Fujii and J.-M. Lehn, *Chem. Commun.*, 2007; N. Iwasawa and H. Takahagi, *J. Am. Chem. Soc.*, 2007, **129**, 7754; M. Hutin, C. J. Cramer, L. Gagliardi, A. R. M. Shahi, G. Bernardinelli, R. Cerny and J. R. Nitschke, *J. Am. Chem. Soc.*, 2007, **129**, 8774–8780; C. D. Pentecost, K. S. Chichak, A. J. Peters, G. W. V. Cave, S. J. Cantrill and J. F. Stoddart, *Angew. Chem., Int. Ed.*, 2007, **46**, 218–222; P. C. Haussmann, S. I. Khan and J. F. Stoddart, *J. Org. Chem.*, 2007, **72**, 6708–6713; F. Dumitru, E. Petit, A. van der Lee and M. Barboiu, *Eur. J. Inorg. Chem.*, 2005, 4255–4262; P. N. W. Baxter, J.-M. Lehn and K. Rissanen, *Chem. Commun.*, 1997, 1323–1324.
- 17 N. Giuseppone and J.-M. Lehn, *Angew. Chem., Int. Ed.*, 2006, **45**, 4619–4624.
- 18 A. Zhu, M. J. Mio, J. S. Moore and H. G. Drickamer, *J. Phys. Chem. B*, 2001, **105**, 3300–3305.
- 19 A. V. Eliseev and M. I. Nelen, *Chem.–Eur. J.*, 1998, **4**, 825–834; A. V. Eliseev and M. I. Nelen, *J. Am. Chem. Soc.*, 1997, **119**, 1147–1148.
- 20 V. Berl, M. J. Krische, I. Huc, J.-M. Lehn and M. Schmutz, *Chem.–Eur. J.*, 2000, **6**, 1938–1946; V. Berl, I. Huc, J.-M. Lehn, A. DeCian and J. Fischer, *Eur. J. Org. Chem.*, 1999, 3089–3094.
- 21 D. H. Busch, *Templates in Chemistry II*, Springer-Verlag, Berlin Heidelberg, 2005.
- 22 S. M. Nelson, *Pure Appl. Chem.*, 1980, **52**, 2461–2476.
- 23 R. L. E. Furlan, S. Otto and J. K. M. Sanders, *Proc. Natl. Acad. Sci. U. S. A.*, 2002, **99**, 4801–4804.
- 24 U. Luning, *J. Inclusion Phenom. Macrocyclic Chem.*, 2004, **49**, 81–84; O. Storm and U. Luning, *Chem.–Eur. J.*, 2002, **8**, 793–798.
- 25 M. J. Marsella, H. D. Maynard and R. H. Grubbs, *Angew. Chem., Int. Ed. Engl.*, 1997, **36**, 1101–1103.
- 26 S. Yagai, T. Karatsu and A. Kitamura, *Chem.–Eur. J.*, 2005, **11**, 4054–4063.
- 27 P. Kuad, A. Miyawaki, Y. Takashima, H. Yamaguchi and A. Harada, *J. Am. Chem. Soc.*, 2007, **129**, 12630–12631; F. Rakotondrandany, A. Whitehead, A. M. Lebus and H. F. Sleiman, *Chem.–Eur. J.*, 2003, **9**, 4771–4780; M. S. Vollmer, T. D. Clark, C. Steinem and M. R. Ghadiri, *Angew. Chem., Int. Ed.*, 1999, **38**, 1598–1601; S. Shinkai, T. Yoshida, O. Manabe and Y. Fuchita, *J. Chem. Soc., Perkin Trans. 1*, 1988, 1431–1437; S. Shinkai, M. Ishihara, K. Ueda and O. Manabe, *J. Chem. Soc., Perkin Trans. 2*, 1985, 511–518.
- 28 *Molecular Switches*, ed. B. L. Feringa, Wiley-VCH, Weinheim, 2001.
- 29 S. Ulrich and J.-M. Lehn, *Angew. Chem., Int. Ed.*, 2008, **47**, 2240–2243.
- 30 G. Ercolani, L. Mandolini, P. Mencarelli and S. Roelens, *J. Am. Chem. Soc.*, 1993, **115**, 3901–3908.
- 31 K. M. Gardinier, R. G. Khoury and J.-M. Lehn, *Chem.–Eur. J.*, 2000, **6**, 4124–4131.
- 32 J. F. Geldard and F. Lions, *Inorg. Chem.*, 1963, **2**, 270–282; H. A. Goodwin and F. Lions, *J. Am. Chem. Soc.*, 1959, **81**, 6415–6422; F. Lions and K. V. Martin, *J. Am. Chem. Soc.*, 1957, **79**, 2733–2738.
- 33 A. M. Stadler, N. Kyritsakas, R. Graff and J.-M. Lehn, *Chem.–Eur. J.*, 2006, **12**, 4503–4522; A. M. Stadler, N. Kyritsakas and J.-M. Lehn, *Chem. Commun.*, 2004, 2024–2025; M. Barboiu and J.-M. Lehn, *Proc. Natl. Acad. Sci. U. S. A.*, 2002, **99**, 5201–5206.
- 34 A. Petitjean, R. G. Khoury, N. Kyritsakas and J.-M. Lehn, *J. Am. Chem. Soc.*, 2004, **126**, 6637–6647; S. Ulrich and J.-M. Lehn, unpublished results.
- 35 C. D. Meyer, C. S. Joiner and J. F. Stoddart, *Chem. Soc. Rev.*, 2007, **36**, 1705–1723.
- 36 D. Schultz and J. R. Nitschke, *J. Am. Chem. Soc.*, 2006, **128**, 9887–9892.
- 37 N. Giuseppone, J.-L. Schmitt, E. Schwartz and J.-M. Lehn, *J. Am. Chem. Soc.*, 2005, **127**, 5528–5539.
- 38 D. B. Dess and J. C. Martin, *J. Org. Chem.*, 1983, **48**, 4155–4156.
- 39 J. L. Schmitt, A. M. Stadler, N. Kyritsakas and J.-M. Lehn, *Helv. Chim. Acta*, 2003, **86**, 1598–1624.
- 40 S. T. Howard, *J. Am. Chem. Soc.*, 1996, **118**, 10269–10274.
- 41 The correlation between H₂ and H₆ is not always seen because in some cases the NMR signals of those protons are very close. The correlation would then be very close to the diagonal and is probably hidden by signal noise.
- 42 U. S. Schubert, G. R. Newkome and H. Hofmeier, *Modern Terpyridine Chemistry*, Wiley-VCH Verlag, Weinheim, 2006.
- 43 R. S. Macomber, *A Complete Introduction to Modern NMR Spectroscopy*, Wiley Interscience, New York, 1998; J. B. Lambert and E. P. Mazzola, *Nuclear Magnetic Resonance Spectroscopy*, Pearson Education Inc., Prentice Hall, 2003.
- 44 L. G. Sillen and B. Warnqvist, *Ark. Kemi.*, 1969, **31**, 377–390.
- 45 A. Bencini, A. Bianchi, P. Dapporto, E. Garcia-España, M. Micheloni and P. Paoletti, *Inorg. Chem.*, 1989, **28**, 1188–1191; F. Amaud-Neu, B. Spiess and M. J. Schwing-Weill, *J. Am. Chem. Soc.*, 1982, **104**, 5641–5645; J.-M. Lehn and J.-P. Sauvage, *J. Am. Chem. Soc.*, 1975, **97**, 6700–6707; B. Dietrich, J.-M. Lehn and J.-P. Sauvage, *Tetrahedron*, 1973, **29**, 1647–1658.
- 46 J. R. Nitschke, *Acc. Chem. Res.*, 2007, **40**, 103–112.
- 47 C. Godoy-Alcantar, A. K. Yatsimirsky and J.-M. Lehn, *J. Phys. Org. Chem.*, 2005, **18**, 979–985.
- 48 B. Levrand, W. Fieber, J.-M. Lehn and A. Herrmann, *Helv. Chim. Acta*, 2007, **90**, 2281–2314.
- 49 V. A. Polyakov, M. I. Nelen, N. Nazarpak-Kandlousy, A. D. Ryabov and A. V. Eliseev, *J. Phys. Org. Chem.*, 1999, **12**, 357–363.
- 50 These values were obtained from peak integrations from ¹H NMR data.
- 51 J. A. Thomas, *Chem. Soc. Rev.*, 2007, **36**, 856–868.
- 52 S. Zameo, B. Vauzeilles and J. M. Beau, *Eur. J. Org. Chem.*, 2006, 5441–5444.
- 53 F. Arico, T. Chang, S. J. Cantrill, S. I. Khan and J. F. Stoddart, *Chem.–Eur. J.*, 2005, **11**, 4655–4666.
- 54 S. Trimpin, A. C. Grimsdale, H. J. Rader and K. Mullen, *Anal. Chem.*, 2002, **74**, 3777–3782; R. Skelton, F. Dubois and R. Zenobi, *Anal. Chem.*, 2000, **72**, 1707–1710.
- 55 G. Ercolani, M. Ioele and D. Monti, *New J. Chem.*, 2001, **25**, 783–789; G. Ercolani, *J. Phys. Chem. B*, 1998, **102**, 5699–5703; X. Chi, A. J. Guerin, R. A. Haycock, C. A. Hunter and L. D. Sarson, *Chem. Commun.*, 1995, 2563–2565.
- 56 C. Schmuck, T. Rehm, L. Geiger and M. Schafer, *J. Org. Chem.*, 2007, **72**, 6162–6170; S. Schlund, C. Schmuck and B. Engels, *Chem.–Eur. J.*, 2007, **13**, 6644–6653.
- 57 T. Ono, T. Nobori and J.-M. Lehn, *Chem. Commun.*, 2005, 1522–1524; W. G. Skene and J.-M. P. Lehn, *Proc. Natl. Acad. Sci. U. S. A.*, 2004, **101**, 8270–8275.
- 58 J. L. Mynar and T. Aida, *Nature*, 2008, **451**, 895–896; P. Cordier, F. Tournilhac, C. Soulie-Ziakovic and L. Leibler, *Nature*, 2008, **451**, 977–980; S. D. Bergman and F. Wudl, *J. Mater. Chem.*, 2008, **18**, 41–62; X. X. Chen, M. A. Dam, K. Ono, A. Mal, H. B. Shen, S. R. Nutt, K. Sheran and F. Wudl, *Science*, 2002, **295**, 1698–1702; P. Reutenauer and J.-M. Lehn, unpublished results.
- 59 A. Macchioni, G. Ciancaleoni, C. Zuccaccia and D. Zuccaccia, *Chem. Soc. Rev.*, 2008, **37**, 479–489; N. Giuseppone, J. L. Schmitt, L. Allouche and J.-M. Lehn, *Angew. Chem., Int. Ed.*, 2008, **47**, 2235–2239; L. Allouche, A. Marquis and J.-M. Lehn, *Chem.–Eur. J.*, 2006, **12**, 7520–7525; Y. Cohen, L. Avram and L. Frish, *Angew. Chem., Int. Ed.*, 2005, **44**, 520–554.
- 60 E. Buhler, S. J. Candau, J. Schmidt, Y. Talmon, E. Kolomiets and J.-M. Lehn, *J. Polym. Sci., Part B: Polym. Phys.*, 2007, **45**, 103–115; E. Buhler and F. Boue, *Macromolecules*, 2004, **37**, 1600–1610.

- 61 E. Kolomiets, E. Buhler, S. J. Candau and J.-M. Lehn, *Macromolecules*, 2006, **39**, 1173–1181.
- 62 J. des Cloizeaux, *Macromolecules*, 1973, **6**, 403.
- 63 The precision of the fit between the experiment and the theory is affected by the fact that the experiments provide M_w whereas theoretical values use M_n .
- 64 L. Brunsveld, B. J. B. Folmer, E. W. Meijer and R. P. Sijbesma, *Chem. Rev.*, 2001, **101**, 4071–4097; Y. Hasegawa, M. Miyauchi, Y. Takashima, H. Yamaguchi and A. Harada, *Macromolecules*, 2005, **38**, 3724–3730; E. Buhler, S. J. Candau, J. Schmidt, Y. Talmon, E. Kolomiets and J. M. Lehn, *J. Polym. Sci., Part B: Polym. Phys.*, 2007, **45**, 103–115.
- 65 Y. Okada and F. Tanaka, *Macromolecules*, 2006, **39**, 8153–8162; A. Ciferri, in *Supramolecular Polymers*, ed. A. Ciferri, Taylor and Francis Group, 2005.
- 66 S. Masiero, S. Lena, S. Pieraccini and G. P. Spada, *Angew. Chem., Int. Ed.*, 2008, **47**, 3184–3187.
- 67 P. Dechambenoit, S. Ferlay, M. W. Hosseini, J. M. Planeix and N. Kyritsakas, *New J. Chem.*, 2006, **30**, 1403–1410; F. Qian, J. E. McCusker, Y. Zhang, A. D. Main, M. Chlebowsky, M. Kokka and L. McElwee-White, *J. Org. Chem.*, 2002, **67**, 4086–4092.
- 68 H. E. Gottlieb, V. Kotlyar and A. Nudelman, *J. Org. Chem.*, 1997, **62**, 7512–7515.
- 69 M. Lazarte, A. C. G. Marigliano and H. N. Solimo, *J. Solution Chem.*, 2004, **33**, 1549–1563; H. Kovacs, J. Kowalewski and A. Maliniak, *J. Phys. Chem.*, 1989, **93**, 962–969.
- 70 R. Ziessel, P. Nguyen, L. Douce, M. Cesario and C. Estournes, *Org. Lett.*, 2004, **6**, 2865–2868.
- 71 D. W. Cai, D. L. Hughes and T. R. Verhoeven, *Tetrahedron Lett.*, 1996, **37**, 2537–2540.